NADPH oxidase: A Possible Therapeutic Target for Cognitive Impairment in Experimental Cerebral Malaria

Simhadri Praveen Kumar
University of Hyderabad School of Life Sciences
Prakash Babu Phanithi (prakash@uohyd.ac.in)
University of Hyderabad https://orcid.org/0000-0002-4634-9967

Research Article

Keywords: NADPH oxidase 2, apocynin adjunctive therapy, hippocampal neuronal density, long-term cognitive impairment

Posted Date: June 7th, 2021

DOI: https://doi.org/10.21203/rs.3.rs-549894/v1

Version of Record: A version of this preprint was published at Molecular Neurobiology on November 16th, 2021. See the published version at https://doi.org/10.1007/s12035-021-02598-1.

Abstract

Long-term cognitive impairment associated with seizure-induced hippocampal damage is the key feature of cerebral malaria (CM) pathogenesis. One-fourth of child survivors of CM suffer from long-lasting neurological deficits and behavioral anomalies. However, mechanisms on hippocampal dysfunction are unclear. In this study, we elucidated whether gp91phox isoform of Nicotinamide Adenine Dinucleotide Phosphate oxidase 2 (NOX2) (a potent marker of oxidative stress) mediates hippocampal neuronal abnormalities and cognitive dysfunction in experimental CM (ECM). Mice symptomatic to CM were rescue treated with artemether monotherapy (ARM) and in combination with apocynin (ARM + APO) adjunctive based on scores of Rapid Murine Come behavior Scale (RMCBS). After a 30 day survivability period, we performed Barnes maze, T-maze, novel object recognition cognitive tests to evaluate working and reference memory in all the experimental groups except CM. Sensorimotor tests were conducted in all the cohorts to assess motor coordination. We performed Golgi-cox staining to illustrate cornu ammonis-1 (CA1) pyramidal neuronal morphology and study changes in overall hippocampal neuronal density. Further, expression of NOX2 and NeuN (a neuronal marker) in hippocampal CA1, dentate gyrus was determined using double immunofluorescence experiments in all the experimental groups. Mice administered with ARM monotherapy and APO adjunctive treatment exhibited similar survivability. The latter showed better locomotor and cognitive functions, reduced ROS levels, and hippocampal NOX2 immunoreactivity in ECM. Our results show a substantial increase in hippocampal NeuN immunoreactivity and dendritic arborization in ARM + APO cohorts compared to ARM-treated brain samples. Overall, our study suggests that overexpression of NOX2 could result in loss of hippocampal neuronal density and dendritic spines of CA1 neurons affecting the spatial working and reference memory during ECM. Notably, ARM + APO adjunctive therapy reversed the altered neuronal morphology and oxidative damage in hippocampal neurons restoring long-term cognitive functions after CM.

Introduction

Malaria remains one of the most important infectious diseases till date. About 409,000 deaths were estimated globally in the year 2019, of which 86 % cases were accounted from Africa and India (World malaria report 2020) and 1 % of them progress to cerebral malaria (CM) [1]. CM is a neurodegenerative disease, classified under the severe forms of malaria, caused by the infection of *Plasmodium falciparum* exhibiting fatal complications such as recurrent seizures, delirium, and coma, ultimately leading to death [2]. Loss of cognition and behavior after treatment is one of the salient features of CM. Previous reports show that 25 % of children exhibit long-term cognitive impairment after survival from CM [1]. The mechanism underlying the cognitive decline is not known.

Reactive oxygen species (ROS) are the oxygen-derived reactive molecules, essential for the maintenance of several biological processes such as cell growth, survival, differentiation and immune response [3,4]. Several reports show that nicotinamide adenine dinucleotide phosphate (NADPH) oxidase (NOX), a multi-subunit enzyme, generates ROS for maintaining host immunity and physiological processes in the brain [5,6]. NOX consists of seven isoforms NOX1-5, dual oxidases 1–2 (DUOX1) and DUOX2 which combine to form a functional enzyme constituting cytosolic subunits p47-phox, p67-phox, p40-phox, Rac and membrane bound subunits gp91-phox and p22-phox [6,7,5]. Most of the studies reported that increased expression of NOX leads to oxidative damage induced cognitive impairment and loss of motor co-ordination in Alzheimer's and Parkinson diseased patients [8,9]. Increased gp91-phox expression of NOX2 subunit produces superoxides resulting in oxidative stress and inflammatory actions implicated in several neurodegenerative diseases [10–13]. Excessive release of

free radicals results in oxidative stress enhancing hippocampal lesions followed by neurocognitive sequelae in CM [14–17].

Inhibition of NOX has shown an effective response in restoration of neuronal functions in several acute and chronic CNS disorders [8,18,19]. Apocynin (APO), a potent inhibitor of NOX, has multiple therapeutic effects such as anti-oxidant, an anti-inflammatory which is proven to show neuroprotection in several animal models of neurodegeneration [20,19]. Artemisinin derivates are considered the first-line therapy in human cerebral malaria (HCM) [21,22]. In the present study, we administered APO in combination with artemether (APO + ARM) adjunctive therapy and ARM drug (monotherapy) to two different cohorts of C57BL/6 mice infected with *Plasmodium berghei* ANKA (PbA), a widely accepted animal model for CM. Further, we conducted cognitive tests to study the sensorimotor functions, working and long-term memory in all the treated animals in comparison to the control. This study shows the first evidence that apocynin adjunctive therapy was able to decrease the expression of hippocampal NOX2 with improvement in learning and memory functions after CM.

Materials And Methods

Animals

A total of 80 C57BL/6 male and female mice of 3–4 weeks old of 15–20 g were purchased from the National Institute of Nutrition (NIN), Hyderabad. All the animals were fed with chow and sterile water *ad libitum* followed by 12 hours light / dark cycle in the animal house facility at the University of Hyderabad.

Parasite infection and evaluation of symptoms of CM

Mice were infected intraperitoneally (i.p.) with 100–350µl of PbA infected red blood corpuscles (iRBC's) at a concentration of 10^6 was obtained from the National Institute of Malaria Research (NIMR), New Delhi and stored in liquid nitrogen. The PbA infected vials were thawed at 4 ^{0}C and diluted in 1x phosphate buffered saline (PBS) for administration into the mice (n = 15/group). All the infected mice were segregated into 3 groups (CM infected; ARM + APO adjunctive therapy; ARM monotherapy). The parasitemia from the caudal blood smears was monitored by Giemsa staining after 72 hours post-infection. Each mouse was subjected to Rapid Murine Coma Behavior Scale (RMCBS), a tool for identifying the subjects of CM and performing rescue treatment. RMCBS experiment consists of 10 behavioral parameters; gait, balance, motor performance, body position, limb strength, touch escape, pinna reflex, toe pinch, aggression, grooming. Each parameter was scored from 0–2 depending on the behavior exhibited by an infected mouse considering a total score of 20. Mice with scores ranging from 5–12 were considered as symptomatic to CM and subjected to treatment.

Experimental groups

Animals symptomatic to CM was administered (i.p.) immediately with ARM at a concentration of 25 mg/Kg body weight (b.w.) of ARM (dissolved in Arachis oil) and APO at 5mg/Kg (b.w.) (dissolved in 10 % of dimethyl sulphoxide (DMSO) once per day up to seven days. All the animals that received the adjunctive therapy were transferred to a separate cage labeled as ARM + APO group (n = 23). Another cohort of CM infected animals (n = 16) were administered i.p. with 25 mg/kg (b.w.) artemether and transferred to a cage labeled as ARM group (n = 27). Control mice (CON) (n = 15) were administered with saline. Animals symptomatic to CM were categorized as CM infected group (n = 11), which were euthanized humanely with ketamine (150 mg/kg) and xylazine (10

mg/kg) i.p. on day 6–11. All the treated animals were subjected to cognitive tests after a survival period of 30 days and euthanized for brain sampling.

Behavioral tests

Animals with mild CM symptoms (n = 11) were tested immediately for spontaneous activity (cylinder and adhesive removal test). Memory associated tests were performed in the treated animals (ARM n = 15. ARM + APO n = 12) in comparison to CON group after survivability of 30 days. All the tests were performed during the light cycle and analyzed by a group of blinded researchers.

Cylinder test

Each animal from all the experimental groups was placed in a clean, transparent plastic open-top cylinder (height: 26 cm; diameter: 16 cm) and video recorded for 3 minutes. The number of rears (vertical posture of the mouse, standing on its hind limbs) for each mouse was counted. The cylinder was periodically cleaned with 70 % alcohol after each trial. The average number of rears and time spent grooming were measured in all the animal groups.

Adhesive removal test

This test was performed to study the deficits in sensorimotor response to stimulation test adapted for rodents [23–26]. Small pieces of adhesive labels were stuck beneath the toe of the mouse and placed in the cage. Each animal was subjected to three alternative trials with a 2 minute time interval between the tests. If the animal fails to remove adhesive after 120 seconds, the trial was preceded with the next mouse. The average time to contact the adhesive, till its removal from the toe was recorded.

Beam balance test

Each animal (except CM group) was guided to walk from one end of the beam to another (40 cm height, 1 meter beam, 12 mm width) to study the motor deficits [27] for two days and one day for testing. Each mouse received three trials on the test day to analyze the rate of “slipping” (any foot coming off the beam) as a motor deficit with a scoring index of “1” (inability to cross the beam), “2” (crossing the beam with dragging limbs) and “7” (crossing the beam with fewer than 2-foot slips). The beam was cleaned with 70% alcohol, and droppings were removed with clean dry paper.

Barnes maze

This task is performed to evaluate the spatial long-term memory in the rodents [28,29]. This test consists of a circular platform with 20 equidistantly spaced holes along its perimeter (100 cm in diameter). This test consists of a circular platform with 20 equidistantly spaced holes along its perimeter (100 cm in diameter). An escape platform was placed under one of the holes leaving the rest empty. Each animal was guided from the center of the maze to detect escape platform for 4 minutes per session up to 4 days (acquisition phase). The maze and the escape platform were cleaned with 70 % alcohol following each trial. Animals were subjected to probe trial after removing the escape platform on day 5. The time to detect the escape platform (primary latency) and the number of holes entered before primary latency (primary error) were recorded. The mice were video-recorded and tested individually with the ANY-maze behavioral tracking software version 6.0, Stoelting Co, Wood Dale, USA.

T-maze experiment

Mice were subjected to T-maze consisting of three arms measuring (diameter 30 x15 cm height) of left and right sided goal arms and 40 cm of the start arm. A forced choice of spontaneous alternation was selected where each mouse was gently placed in the start arm for 3 minutes for habituation [30–32]. The mouse was placed in the start arm of the maze after blocking any one side of the arm. The mouse is forced to explore the L-shaped maze for 5 minutes (acquisition phase). The mouse was placed back in its home cage for 15 minutes time duration. The maze was cleaned thoroughly with 70 % alcohol to remove olfactory cues in the area. During the test phase, the blockage in the arm was removed, and mouse was placed in the start arm and observed for its entry to the arm not visited previously (correct alternation) (test phase). Mouse exploring the arm visited previously during the test phase is considered as wrong alternation. Each mouse was subjected to 6 trials per day for four days to study the "correct alternation" and "wrong alternation." The percentage of correct alternation per animal with side preference rate (actively adapt to one side of the arm) was calculated and compared among the groups.

One-trial novel object recognition test

On day 1, mouse was placed in the empty square shaped box made of transparent glass material (dimensions: 30 x 30 x 30cm) for 20 minutes (habituation phase). The mouse was removed from the arena and placed back in its home cage. The box was cleaned with 70 % alcohol. On day 2, two identical objects were placed 5 cm away from the walls. Mouse was placed in the box for 5 minutes (familiarization phase). Mouse was placed back in its home cage. The walls of the box along with the identical objects were cleaned thoroughly with 70% alcohol. One of the identical objects was replaced with a novel object having a different shape and colour in same position. After 60 minutes, the same mouse was placed in the center of the arena for 5 minutes (test phase). The total time spent by the subject interacting with both the identical objects in the familiarization and novel object in test phase via. sniffing, pawing, within a distance of 2 cm was recorded manually [33]. The discrimination ratio was calculated to estimate the preference towards novel object (novel object interaction/ total interaction with both objects x 100.

Histological staining

After conducting behavioral assays, all the animals were euthanized and perfused intracardially with saline and chilled 4% paraformaldehyde solution (PFA). The whole brain samples were collected and stored in 4% PFA. Brain samples were placed in Golgi-Cox stain solution at room temperature for 17 days. The rest of the brain samples were dehydrated in 20–40 % sucrose solutions followed by cryomicrotomy. Hippocampal sections of 10 µm thickness were collected to perform immunofluorescence, Fluoro-Jade C and Hematoxylin and Eosin (H&E) staining, 100 µm sections for Golgi-Cox staining. We assessed the changes in the CA1 and Dentate gyrus regions of hippocampus in all the experimental groups.

Fluoro-Jade C staining

Hippocampal brain sections were subjected to the Fluoro-Jade C staining, an anionic dye (AG325 Millipore) which stains only the degenerated neurons [34]. All the sections were immersed in xylene for 45 minutes and dehydrated in 100% ethyl alcohol with 5% sodium hydroxide for 5 minutes. All the sections were washed in phosphate buffer saline (PBS) buffer for 2 minutes and incubated in 0.06% potassium permanganate solution

for 10 minutes with gentle shaking. All the slides were placed in of Fluoro-Jade C stain (FJ-C) solution (0.05% of Fluoro-Jade C powder dissolved in distilled water with 50 µl of acetic acid) for 20 minutes. All the sections were washed with distilled water for 2 minutes, dried at 50 ^{0}C at dark for 15 minutes and mounted with DPX mounting medium. The number of FJ-C positive neurons was quantified by the cell counter tool of Image J software.

Hematoxylin and Eosin (H&E) staining

H&E staining is a standard and well established method for studying morphological changes in tissues during various pathological conditions [35]. All the brain sections were stained with the Harris hematoxylin stain according to the protocols mentioned previously [36–38]. All the images were captured using the Olympus BX-51 microscope at 1000X magnification.

Golgi-Cox staining

Sucrose dehydrated whole brains impregnated with Golgi-Cox stain was subjected to cryosectioning using Leica Cryomicrotome CM 1850. Hippocampal brain sections were collected at 100µm thickness for studying the dendritic spine density and 200 µm to analyze the neuronal arborization pattern by Sholl analysis. The cryosections were developed according to the protocol of Sami Zaquot et al. [39]. All the images were captured by the Olympus BX-51 microscope at 1000X and 400X magnification.

Quantification of dendritic spine density of hippocampal CA1 pyramidal neurons

Dendritic spines were quantified from the skeletonized images of Golgi impregnated CA1 neurons using the cell counter tool of ImageJ software. Spine projections per 10 µm dendrite length of eighteen distal dendrites were considered for quantification from Golgi impregnated CA1 neuronal images captured at 1000X magnification using Olympus BX-51 microscope.

Sholl analysis of hippocampal CA1 pyramidal neurons

Neuronal arborization pattern was quantified by selecting the widely used linear method of the Sholl analysis algorithm [40]. Sholl analysis draws imaginary concentric circles overlapping from soma of the neurons. A highly arborized neuron develops more intersections compared to an altered neuron. The number of intersections (Nm), radius at maximum Nm is critical radius (r_c), number of primary dendrites (Np) were calculated using Sholl plugin of ImageJ software. The soma centered hippocampal pyramidal neurons (n = 16 per group) were converted to 8 bit binary, skeletonized and subjected to threshold. The image was subjected to Sholl plugin after drawing a line from the soma to the border of the image. Based on the linear Sholl plot, a graph was plotted for average values of Nm on Y-axis against r_c on X-axis for each experimental group. Further, we measured the number and total length of apical and basal dendrites of Golgi-impregnated CA1 neurons (n = 16) in all experimental groups by the Neuron J plugin 1.4.3 tool in ImageJ software.

Evans Blue staining

Cohorts of ARM (n = 3), ARM + APO (n = 3) on day 13, CM infected (n = 3) on day 7 and CON (n = 3) mice were injected intravenously (i.v.) with 2 ml/kg of 2% Evans Blue dye (SRL Chemicals 46650). Mice were anesthetized with ketamine (150 mg/kg), xylazine (10 mg/kg) and perfused intracardially with 1x PBS buffer after an hour. Brains were surgically removed, weighed and immersed in 1 ml of formamide solution for 48 hours at 37 ^{0}C. The

samples were homogenized and centrifuged at 14,000 rpm for 20 minutes at 20 ^{0}C. Supernatants were collected carefully and absorbance was measured at 620 nm using UV-visible spectrophotometer (Hitachi–U2900). The amount of the dye (microgram per milligram of tissue) extravasated was quantified by measuring the absorbance of the dye from the brain samples compared to the standard values of Evans blue dye.

Semi-quantitative PCR

Total RNA was isolated from the whole brain samples of all the experimental groups (n = 4 per group) using Trizol reagent (T9424 Sigma Aldrich) and quantified using NanoDropTM 2000 UV-Visible spectrophotometer (Thermo Fisher Scientific). cDNA was synthesized from the 1µg concentration of RNA using PrimeScript™ 1st strand cDNA Synthesis kit (6110A Takara Bio). cDNA at 0.5µg/µl (0.5 µl) concentration, 10 picomolar concentration of forward, reverse primers (1µl) were added to 5 µl of 2x Dreamtaq green PCR master mix (K1081 Thermo Fisher Scientific), made up to 10µl reaction with 3.5 µl of nuclease-free water and subjected to semi-quantitative PCR (Applied Biosystems Veriti 96 well Thermal cycler) at 25 cycles respectively. PCR protocol included denaturation step at 95 ^{0}C for 30 seconds (stage-1), 95 ^{0}C for 2 minutes (stage-2), annealing at respective melting temperature (Tm) for 45 seconds and extension at 72 ^{0}C for 5 minutes. Primers were procured from Integrated DNA Technologies (IDT). Primer sequences specific to NOX2 and GAPDH genes are listed in table 1.

Estimation of ROS by 2, 7-dichlorodihydrofluorescein diacetate (DCFDA) method

2',7'-Dichlorofluorescin diacetate (Sigma Aldrich D6883) is a non-fluorescent probe used to estimate the cellular ROS levels involving hydrogen peroxide (H_2O_2), hydroxyl radicals (OH^-) and peroxyl radicals (ROO^-). De-esterification of DCFDA intracellularly leads to the formation of a highly fluorescent compound, 2',7'-dichlorofluorescein. Whole brain samples (100 mg) (n = 6) were homogenized in 1x PBS buffer in a Dounce homogenizer and centrifuged for 6000 rpm at 4 ^{0}C for 15 minutes. 55 µl of HEPES buffer was mixed to 10 µl of the supernatant. 20 µM of DCFDA was dissolved in the culture grade dimethylsulphoxide (DMSO) solution was added to the above mixture in a 96 well plate and kept for incubation for 30 minutes at room temperature at dark condition. Hydrogen peroxide (100µM in PBS) was used as a positive control. Mean Relative Fluorescence Units (RFU) were measured at an excitation wavelength of 485 nm and emission wavelength of 515 nm of Tecan Infinite 200 PRO spectrofluorometer.

Western blotting

The whole brain samples were homogenized in sucrose radio-immunoprecipitation assay buffer (RIPA) buffer (10 mM Tris-HCl, 0.32 M sucrose, 150 mM NaCl, 1 % NP-40, 0.5 % sodium deoxycholate, and pH-7.2) with 10 µl per 1 ml of protease inhibitor (P0044 Sigma-Aldrich) using a Dounce homogenizer at 4 ^{0}C. The protein extracts were estimated by Bradford method and 50 µg of proteins were resolved in 10 % Sodium-Dodecyl Sulphate-Poly Acrylamide Gel Electrophoresis (SDS-PAGE) gel. The resolved gel were blotted on the nitrocellulose membrane soaked in Towbin buffer (Tris-HCl- 3 g, glycine-14.4 g, deionized water – 800 ml, methanol – 200 ml pH-8.3) overnight at 4 ^{0}C. The membranes were blocked in 5 % skimmed milk buffer for 1 hour at room temperature and washed with Tris-buffered saline containing 0.05 % Tween 20 (TBST) for 5 minutes. Membrane was incubated with primary antibodies of NOX2 rabbit raised polyclonal antibody (Abcam ab80508) and GAPDH (#5174, Cell Signaling Technology) at dilution of 1:1000 overnight at 4 ^{0}C. The membrane was washed with TBST and

probed with anti-rabbit IgG (1:30,000) (whole molecule) (A3687 Sigma-Aldrich) alkaline phosphatase conjugated secondary antibody for 2 hours at room temperature. Immunoreactivity was detected by adding 120 µl of BCIP solution (5-bromo-4-chloro-3-indolyl-phosphate) (75531 SRL chemicals), 120 µl of NBT solution (Nitro Blue Tetrazolium) (73654 SRL chemicals) to 4ml of alkaline phosphatase buffer (Tris-2.422 g, NaCl- 1.68 g and MgCl2- 0.203 g dissolved in 200 ml of distilled water) on the membrane for 5–10 minutes at room temperature in dark condition.

Double immunofluorescence experiment

Hippocampal brain sections were permeabilized with 0.2 % Tween for 20 minutes. All the sections were blocked using blocking buffer (5 % normal goat serum (Cell Signaling Technology, #5425) dissolved in 1x PBS) for 2 hours at room temperature. Sections were incubated with the primary antibody cocktail of rabbit generated anti-NOX2/gp91phox antibody (1:100) (Abcam, ab80508) and mouse raised NeuN (neuronal marker) antibody (1:100) (Cell Signaling Technology, #94403) overnight for 16 hours at 4^0C. Sections were rinsed in 1x PBS and incubated with a secondary antibody cocktail of anti-rabbit IgG (1:1000) (4412S Alexa Fluor® 488 Conjugate) and anti-mouse IgG (1:1000) (4409S Alexa Fluor® 555 Conjugate) from Cell Signaling Technology for 2 hours at room temperature in dark condition. After washing the sections in 1x PBS, the sections were mounted with Prolong Gold Anti-Fade reagent with DAPI (8961S Cell Signaling Technology). Images were captured by the Carl Zeiss LSM 710 confocal microscope using ZEN Blue software. The fluorescence intensities of images were quantified by the ImageJ software (n = 8 images per group).

Statistical analysis

The statistical differences among the experimental groups were calculated by one-way ANOVA (Analysis of Variance) with post-hoc Student-Newman-Keuls test (multiple comparisons) using the GraphPad Prism software version 5.03. The p-values less than 0.05 and 0.001 were considered significant.

Results

Rescue therapy with ARM and ARM + APO improves behavioral patterns after ECM.

We observed that the mice infected PbA showed altered behavior from day 5 such as loss of rearing and exploration (60 seconds for exploring the corners) with an RMCBS score of 12 ± 1. Later, most of the PbA infected mice were insensitive to touch escape, pinna reflex, with a sharp decline in the RMCBS score from day 6–9 (day 6; 11 ± 0.57, day 7; 6.33 ± 0.88, day 8; 5.3 ± 0.3, day 9; 5 ± 0.57) (Supplementary 1). We administered ARM drug to a cohort of PbA infected mice at RMCBS score of 14 i.e. from day 6 (ARM group, n = 27) (Supplementary 2). Mice were administered with APO + ARM at a RMCBS score of 14 i.e. from day 6 (n = 23) (Fig. 1a, c). ARM group exhibited an improvement in behavioral patterns from day 9 (RMCBS scores day 8; 15.33 ± 1.2, day 9; 16.66 ± 0.33, day 10; 17.0 ± 0.57) such as exploration (9 seconds for exploring all the corners), grooming, rearing and subtle deficits in touch response, body balance and locomotion compared to CM group. ARM + APO treated group also exhibited improvement in gait, grooming pattern, prompt response to pinna reflex and touch response (RMCBS scores of ARM + APO group (day 8; 14.33 ± 0.33. day 9; 17.33 ± 0.33; day 10; 17.0 ± 0.57) (supplementary 3) compared to CM group. Exploration rate of ARM + APO and ARM treated mice (8 seconds for exploring all the corners) were similar. CON group (n = 15) exhibited typical behavioral response with

RMCBS score of 20 (supplementary 4). We observed that the survival rate in both the groups was similar. Mice treated with ARM showed a survival rate of 56 %, ARM + APO group of 54 % survivability on day 30 (Figure. 1b). Mice rescue treated with ARM + APO died of parasite recrudescence on day 11 and 12, day 10. Some of the ARM treated mice died few hours after receiving treatment. Mice symptomatic to CM were moribund between day 6 to 9.

Apocynin adjunctive therapy improved cytoarchitecture of hippocampal neurons in ECM

The H&E stained sections of CM infected group illustrated characteristic neurodegenerative changes such as irregularly shaped or shrunken necrotic CA1 neurons with pyknotic nucleus (Fig. 2a). We observed prominent increase in neuropil vacuolation in the internal granule layer and hilus of dentate gyrus in CM group. A reduction in number of pyknotic neurons with vacuolar changes in the neuropil was observed in CA1 and dentate gyrus of ARM + APO group compared to ARM rescue treated group (Fig. 2b). FJ-C staining revealed severe neurodegeneration in the CA1 (38 ± 3.0) (Fig. 3a and c) and the granule layer of the dentate gyrus (30.5 ± 4.5) in CM brain sections. ARM treated group showed abundant FJ-C positive neurons in hilus and internal granule layer of the dentate gyrus (26 ± 2) compared to the APO (10.5 ± 1.5) group (Fig. 3b and d). Overall, both the rescue treatments prevented neuronal death after CM, ARM + APO treatment (***$p < 0.001$) showed significant neuroprotection in dentate gyrus and CA1 neurons (*$p < 0.05$) compared to ARM monotherapy in ECM.

Apocynin rescue treatment improves hippocampal CA1 pyramidal neuronal morphology and dendritic spine density in ECM

Our results show critical loss of hippocampal CA1 dendritic complexity in CM infected brain sections (Fig. 4a). Based on the outcomes of H&E, FJ-C staining, we studied whether ARM and ARM + APO treatment had any positive effect on the dendritic arborization and dendritic spine density of CA1 neurons. Both ARM and ARM + APO therapy improved hippocampal dendritic complexity compared to CM infected brain sections (Fig. 4a). Sholl analysis studies demonstrated a significant increase in dendritic arborization and primary dendrites of CA1 neurons in ARM + APO (Nm; 14.24 ± 0.60) at r_c =200 µm, Np = 4.42 ± 0.37 compared to ARM (Nm; 11.04 ± 0.53) at r_c=250 µm, Np = 3.98 ± 0.21 and CM (Nm; 4.96 ± 0.08) at r_c=50 µm, Np = 2.67 ± 0.02). We observed an increased dendritic arborization pattern in CON group (Nm; 16.30 ± 0.9) at r_c=100 µm (Np = 5.02 ± 0.05) (Fig. 4b and d) in comparison to rest of the experimental groups. Golgi-cox impregnated CA1 neurons illustrated significant increase in the number and length of basal dendrites in ARM + APO (BsD number;12.5 ± 1.5, length:438.0 ± 49 µm) (***$p < 0.001$) compared to ARM group (BsD number; 4.5 ± 0.5, length:73.0 ± 16 µm) (Fig. 4e and f) and CM group which exhibited dystrophic neurites (BsD: 3.5 ± 0.5, length: 53.5 ± 7.5 µm) as well as length and number of apical (ApD number; 6.5 ± 0.5, length:188.0 ± 12 µm). There was no significant change in the number and length of apical dendrites of ARM and ARM + APO group. We observed a prominent increase in number and length of apical and basal dendrites in CON group (ApD number: 26.0 ± 2, length: 1915.5 ± 18.5 µm, BsD number: 18.5 ± 1.5, length: 700.5 ± 82.5 µm) compared to the rest of the experimental groups (Fig. 4e and f). Dendritic spine density data indicated a significant increase in ARM + APO (22 ± 0.34) (***$p < 0.001$) compared to ARM (12.50 ± 0.5) treated and CM group (7.0 ± 0.45) (Fig. 4c and g). Our results show increased dendritic spine density in CON group in comparison to rest of the experimental groups (35.0 ± 0.31). Overall, despite both rescue treatments mitigated CM symptoms, Golgi-cox impregnated brain sections exhibited a significant difference in dendritic complexity, spine density and arborization pattern in ARM + APO treated compared to ARM group.

Apocynin rescue therapy restores the BBB integrity, reduces ROS levels and expression of NOX2 in ECM.

Loss of BBB integrity is a salient feature in the pathogenesis of CM [41,42]. Evans blue dye is a well-known vascular marker that does not cross BBB under physiological conditions but binds to albumin and gets across a leaky BBB [43,44]. Brain symptomatic to CM appeared deep blue with increased concentration of Evans blue (9.50 ± 0.5 µg/g brain tissue), while ARM + APO treated showed a lighter blue coloration with a concentration of 4.5 ± 0.5 µg/g Evans blue dye compared to ARM group (6.1 ± 0.87 µg/g) (Fig. 5a). Overall our findings represent that ARM + APO treated group significantly prevented BBB impairment compared to ARM (*$p < 0.05$) and CM infected group (***$p < 0.001$). We observed lower levels of Evans blue dye in CON group (2 ± 0.03 µg/g).

Recent studies show that deletion of NOX2 gene in animal models show partial neuroprotection from brain ischemia and traumatic brain injury (TBI) [45,11]. Gene expression studies revealed that both ARM mono (1.20 ± 0.07) and ARM + APO (0.619 ± 0.04) adjunctive therapy were successful in reducing the NOX2 gene expression compared to CM group (***$p < 0.001$, 2.38 ± 0.27) upon normalization with Glyceraldehyde 3 phosphate dehydrogenase (GAPDH) loading control (Fig. 5b). Protein expression data was in line with results of NOX2 gene expression normalized with GAPDH (protein) showing significant reduction of NOX2 expression in ARM + APO (0.889 ± 0.0089) compared to ARM (*$p < 0.05$; 1.49 ± 0.09) and CM group (***$p < 0.001$; 2.95 ± 0.28) (Fig. 5c). Overall, the gene and protein levels in whole brain lysates showed reduced expression of NOX2 upon treatment with APO adjunctive therapy compared to ARM group in ECM.

Previous studies show ROS induced pathological changes in vascular endothelial damage in CM [46–48]. Mean RFU values of DCFDA test data show significant reduction of ROS in ARM + APO (23460 ± 2522) (***$p < 0.001$) compared to ARM (41465 ± 1663) and CM group (51461.5 ± 2538) (Fig. 5d). Overall, based on the DCFDA test, we confirm that APO adjunctive therapy is effective in lowering the ROS levels compared to ARM monotherapy in ECM.

Apocynin adjunctive therapy reduces NOX2 expression in CA1 and dentate gyrus of hippocampal sections in ECM

Double immunofluorescence staining illustrated significant decrease in the NOX2 fluorescence in dentate gyrus and CA1 in ARM + APO (***$p < 0.001$, dentate gyrus; 6.48 ± 0.25, CA1; 7.32 ± 0.38) compared to ARM (dentate gyrus; 12.36 ± 0.58, CA1; 16.83 ± 0.45) and CM group (dentate gyrus; 16.89 ± 1.12, CA1; 25.47 ± 0.35) (Fig. 6, 7). Loss of NeuN expression is followed by central nervous system (CNS) injury [49–51]. Restoration of NeuN immunoreactivity in dentate gyrus and CA1 regions of hippocampal sections is a clear sign of neuronal recovery in ARM + APO group. We observed a significant loss of NeuN expression was prominent in hilar regions and dentate gyrus in ARM (***$p < 0.001$) compared to ARM + APO group (Fig. 6c). Overall, both rescue therapies were successful in overcoming CM, while ARM + APO treated showed prominent neuroprotection in hippocampal regions compared to ARM group.

Apocynin rescue therapy improves long term memory and restores sensorimotor-coordination after CM.

Our analysis from cylinder test exhibited that the number of rearings was significantly increased in both the rescue treated groups (ARM; 18 ± 1.15 and ARM + APO; 18.33 ± 1.45, ***$p < 0.001$) (Fig. 8a) compared to CM (1.66 ± 0.88). Furthermore, no change in rate of rearings was observed between ARM and ARM + APO treated groups. Adhesive removal test results show a significantly decreased rate of contact 8.5 ± 0.5, removal time 26.5

± 1.5 sec in ARM + APO (***p < 0.001) compared to ARM treated (contact 39.5 ± 5.5, removal time 85.5 ± 4.5, p < 0.001) and CM (contact 88 ± 2, removal time 90.5 ± 0.5 (Fig. 8b and e). Beam balance test results show that ARM group exhibit a characteristic contralateral foot slipping (***p < 0.001, 7.33 ± 0.66) with increase (*p < 0.05) in the average time (11 ± 1.15 sec) (supplementary 5) to traverse the beam compared to ARM + APO group (slipping rate 3.33 ± 0.3, time to traverse 7 ± 1.15 sec) (supplementary 6) (Fig. 8c and f). We observed that CON group occasionally showed slipping and least time to traverse the beam (5.1 ± 0.58 sec) compared to rest of the experimental groups. T-maze spontaneous alternation task results show a significant increase in the rate of correct alternation in ARM + APO (60.0 ± 2.88 %, ***p < 0.001) group compared to ARM group (43.33 ± 6.0 %) (Fig. 8d). We observed that ARM treated (50 ± 2.88 %, ***p < 0.001) group showed a significant strong side preference rate compared to ARM + APO (*p < 0.05) (25.0 ± 2.88 %) and CON group (11.66 ± 1.66) (Fig. 8g). CON group was used as a reference which resulted in 70.66 ± 5.81 % correct alternation rate compared to rest of the groups. Our analysis from Barnes maze experiment revealed that ARM + APO treated group performed primary latency within a shorter time interval (81.76 ± 8.56 sec on day 1 and 16.78 ± 7.9 sec on day 5) (supplementary 7) compared to ARM group (127.0 ± 8.74 sec on day 1 and 37.32 ± 7.46 sec on day 5 during the acquisition phase (Fig. 8h and i) (supplementary 8). The rate of primary errors was increased in ARM treated (29.56 ± 7.5; day 1), (27.0 ± 3.4; day 5) compared to the ARM + APO group (19.00 ± 7.2; day 1), (3.45 ± 2.5; day 5) (Fig. 8j and k). The heat maps show that CON (105.0 ± 5.6 sec) and ARM + APO group (64.56 ± 5.3 sec) spent more time near the escape platform after primary latency compared to the ARM group (34.5 ± 7.9) during probe trial on day 5. Most of the animals in ARM group exhibited frozen behavior in the center of the maze and detected the escape platform upon several nudges (Fig. 8l). Overall, based on the results of Barnes maze, ARM + APO group exhibited better spatial reference memory skills with less error rate compared to the ARM group. Novel object recognition test results revealed that ARM + APO group showed significant increase in the time spent interacting with the novel object (57 ± 2 sec, ***p < 0.001) compared to the ARM group (42.5 ± 2.5 sec) during retrieval phase (Fig. 8m). Further, we observed that there was no significant change in the time spent with two identical objects (object 1 and 2) in all the experimental groups (CON; object 1- 43.5 ± 1.5 sec, object 2- 50.5 ± 2.5 sec, ARM; object 1- 33.5 ± 1.5 sec, object 2- 40.5 ± 2.5 sec, ARM + APO: object 1–36 ± 4 sec, object 2- 42.5 ± 2.5 sec) during acquisition phase (Fig. 8m). Discrimination index percent data represents that ARM + APO (72 %) showed more preference for recognizing novel object compared to ARM group (57 %) (Fig. 8n).

Discussion

Excess ROS production and chronic inflammatory mechanisms activating microglia are propellants for unusual micro-environment in the brain leading to oxidative stress and cognitive decline in several neurodegenerative disorders [52–56]. The pathology of CM includes sequestration of parasite-infected red blood corpuscles (pRBCs) in the micro-vessels of the brain, overexpression of the immune factors causing a breach in the Blood Brain Barrier (BBB) [2,41,57]. Disruption of brain development during childhood may lead to long-lasting consequences on cognition. Generally, cognitive abilities such as learning, attention and memory rapidly develop in children within 8–9 years of age [58]. Loss of CA1 and dentate gyrus neurons in the hippocampus is a major cause for learning and memory impairment in several neurodegenerative diseases [59–61]. Earlier studies showed that children with a history of CM showed hippocampal injury with poor cognitive outcomes [62–64]. A recent MRI report demonstrated bilateral hippocampal sclerosis in HCM with a follow-up of short-term memory loss [65]. However, till date, no effective neuroprotective therapy exists for restoration of cognitive functions after CM.

Superoxides produced by synaptically localized NOX are vital for hippocampal long-term potentiation (LTP) and hippocampal dependent memory formation [66,67]. NOX2 hypersignaling elevates ROS and pro-inflammatory cytokines levels in activated microglial cells in experimental autoimmune encephalomyelitis (EAE) model of multiple sclerosis [68]. However, previous studies have shown a 6–7 fold elevation of NOX2 in CA1 region of hippocampus playing a critical role in the disease progression and altering cognition after transient global cerebral ischemia, Alzheimer's, Parkinson's, Huntington, amyotrophic lateral sclerosis [69–73]. Earlier studies have shown that free radicals synthesized by NOX2 subunit of NADPH oxidase in macrophages do not affect suppressing parasite progression during malaria pathogenesis and have a minimal role in the gp91lphox −/− mice model of malaria [74–76,14]. The current study demonstrates that increased hippocampal NOX2 immunoreactivity is detrimental for hippocampal neurons, negatively affecting learning and memory functions in ECM. However, further research is essential to understand the role of the remaining subunits of NOX in CM pathogenesis.

Existing reports state that NOX subunits alter BBB permeability during neuropathological conditions [77–79]. APO treatment significantly reverses BBB permeability in several animal models of brain injury. Interestingly, several ARM adjunctive therapies are proven to improve BBB integrity, reducing disease pathology in experimental models of CM [42,80,81]. Based on the outcome of Evan's blue experiment, we assume that APO could play an important role in the restoration of BBB integrity after CM. The dosage of 5 mg/Kg APO as in the current study has also been studied for its neuroprotective action in various experimental models of stroke and traumatic brain injury [82–86]. Till date, there are no studies on APO as adjunctive in animal models of CM. ARM is also known for its anti-oxidative, anti-inflammatory, neuroprotective properties [87–89]. Artemisinin derivatives stimulate ROS for mediating cytotoxic action in the parasite [90,91]. Based on the outcomes of our study, we understood that 25mg/kg ARM clears parasite and improves survivability but ineffective in extending neuroprotection after ECM. Interestingly, A.M. Gopalakrishnan group proved that NOX plays a potent role in ROS stimulation in presence of artesunate (one of the artemisinin derivatives) in RBC's infected with *Plasmodium* species [92]. We assume that ARM might exacerbate the oxygenation conditions in the brain, altering neuroprotective signaling mechanisms during rescue therapy. Nevertheless, further research is necessary to study the role of ARM on NOX regarding the maintenance of physiological processes of neurons in the hippocampal circuit in CM.

Changes in dendritic complexity are salient features reported in several neurodegenerative diseases [93–96]. According to previous reports, hippocampal neurons are highly vulnerable to oxidative stress, ischemia and hypoglycemia with characteristic cellular damage [97,98]. Several studies demonstrate that APO acts as a neuroprotective agent inhibiting NOX and microglial activation during pathological conditions [99–101]. Song Hee Lee et al. have shown a significant reduction in hippocampal neuronal death in CA1, CA3, dentate gyrus and hilus regions by APO treatment in pilocarpine-induced epilepsy models [100]. A recent report shows that APO prevented fibrinogen induced dendritic spine loss in cortical neurons and dendritic damage in 5XFAD mouse model of Alzheimer's disease [102]. In our study, ARM + APO rescue treatment increased complexity of hippocampal neuronal density dendritic spine density of CA1 neurons and NeuN immunoreactivity after CM. Therefore, we assume that APO adjunctive modulates NeuN expression triggering neuroprotective signaling mechanisms and accelerating a robust increase in hippocampal dendritic complexity after survival from CM.

Aberrant activation of neuronal NOX dysregulate dopaminergic neurotransmission mediated motor coordination in Parkinson's disease [103]. Recently, our group elucidated mechanism of dysregulation of dopamine receptor

signaling and impairment of striatal medium spiny neurons in ECM [104]. According to various clinical trial reports, children who survived from CM suffer from motor disabilities after ARM treatment [105–108]. Several studies have shown that APO treatment prevented motor deficits in animal models of neurodegeneration [109,103,110]. Our results were in line with the above statement with restoration of locomotor functions after ARM + APO treatment in CM symptomatic animals. However, further research is necessary to elucidate the role of NOX in dysregulation of dopaminergic signaling pathways in the brain responsible for motor coordination in CM pathogenesis. According to Celeste et al., hippocampal lesioned rats exhibit a strong side preference with a lower correct alternation rate revealing short-term memory deficits during the T-maze experiment [111]. Inhibition of NOX2 prevented a decline in spatial memory in aged mice studied by novel object recognition task [112]. Hence, we assume that hippocampal neurodegeneration may correlate to repetitive side preference patterns that contribute to short-term memory loss in the T-maze experiment in ARM group. Despite similar survival rates, we predict that APO counteracts neurotoxicity caused by the ARM in ECM. However, conducting pharmacodynamic drug-drug interactions studies between both drugs in larger groups are essential for understanding the pharmacological effect.

Together, our findings lend strong evidence for NOX2 overexpression in hippocampal regions, upon counteracting with ARM + APO rescue treatment, reduced hippocampal NOX2 expression, restored neuronal arborization, improved cognitive and behavioral functions in ECM. Therefore, we firmly believe APO adjunctive therapy could be a promising therapeutic approach against long-term cognitive impairment after CM.

Declarations

Ethics approval

All the animal experiments were conducted as per the guidelines of the Committee for the Purpose of Control and Supervision of Experimental Animals (CPCSEA), Government of India (Registration No: 48/1999/CPCSEA) after approval from the Institutional Animal Ethics Committee (UH/IAEC/PPB2014-I/68), University of Hyderabad, India.

Funding

The authors wish to acknowledge the financial assistance from Department of Science and Technology Cognitive Science Research Initiative project (DST-CSRI) (Grant No.SR/CSRI/196/2016), Department of Biotechnology (DBT) (Grant No.BT/PR18168/MED/29/1064/2016), Science and Engineering Research Board (SERB) (Grant No.CRG/2020/005021) and INSPIRE student Fellowship (DST/INSPIRE Fellowship/2013/710), Government of India.

Consent for publication

The authors declare that no human subjects were involved in the study.

Data availability statement

All data generated or analyzed during this study are included in this published article (and its supplementary information files).

Conflict of interest

The authors declare that they have no conflict of interest.

Authors' contributions

Simhadri Praveen Kumar designed the hypothesis and experimental methodology. Phanithi Prakash Babu guided and assisted with editing the manuscript.

Acknowledgements

The authors thank Dr. Nakka Venkata Prasuja for sparing apocynin.

Consent to participate

“Not applicable”

References

1. Reis PA, Estato V, da Silva TI, d'Avila JC, Siqueira LD, Assis EF, Bozza PT, Bozza FA, Tibirica EV, Zimmerman GA, Castro-Faria-Neto HC (2012) Statins decrease neuroinflammation and prevent cognitive impairment after cerebral malaria. PLoS pathogens 8 (12):e1003099. doi:10.1371/journal.ppat.1003099
2. Idro R, Marsh K, John CC, Newton CR (2010) Cerebral malaria: mechanisms of brain injury and strategies for improved neurocognitive outcome. Pediatric research 68 (4):267-274. doi:10.1203/00006450-201011001-00524 10.1203/PDR.0b013e3181eee738
3. Yang Y, Bazhin AV, Werner J, Karakhanova S (2013) Reactive oxygen species in the immune system. International reviews of immunology 32 (3):249-270. doi:10.3109/08830185.2012.755176
4. Kohchi C, Inagawa H, Nishizawa T, Soma G (2009) ROS and innate immunity. Anticancer research 29 (3):817-821
5. Nayernia Z, Jaquet V, Krause KH (2014) New insights on NOX enzymes in the central nervous system. Antioxidants & redox signaling 20 (17):2815-2837. doi:10.1089/ars.2013.5703
6. Lambeth JD, Neish AS (2014) Nox enzymes and new thinking on reactive oxygen: a double-edged sword revisited. Annual review of pathology 9:119-145. doi:10.1146/annurev-pathol-012513-104651
7. Lassegue B, Griendling KK (2010) NADPH oxidases: functions and pathologies in the vasculature. Arteriosclerosis, thrombosis, and vascular biology 30 (4):653-661. doi:10.1161/ATVBAHA.108.181610
8. Barua S, Kim JY, Yenari MA, Lee JE (2019) The role of NOX inhibitors in neurodegenerative diseases. IBRO reports 7:59-69. doi:10.1016/j.ibror.2019.07.1721
9. Bruce-Keller AJ, Gupta S, Parrino TE, Knight AG, Ebenezer PJ, Weidner AM, LeVine H, 3rd, Keller JN, Markesbery WR (2010) NOX activity is increased in mild cognitive impairment. Antioxidants & redox signaling 12 (12):1371-1382. doi:10.1089/ars.2009.2823
10. Shahraz A, Wissfeld J, Ginolhac A, Mathews M, Sinkkonen L, Neumann H (2021) Phagocytosis-related NADPH oxidase 2 subunit gp91phox contributes to neurodegeneration after repeated systemic challenge with lipopolysaccharides. Glia 69 (1):137-150. doi:10.1002/glia.23890

11. Dohi K, Ohtaki H, Nakamachi T, Yofu S, Satoh K, Miyamoto K, Song D, Tsunawaki S, Shioda S, Aruga T (2010) Gp91phox (NOX2) in classically activated microglia exacerbates traumatic brain injury. Journal of neuroinflammation 7:41. doi:10.1186/1742-2094-7-41
12. Kumar A, Barrett JP, Alvarez-Croda DM, Stoica BA, Faden AI, Loane DJ (2016) NOX2 drives M1-like microglial/macrophage activation and neurodegeneration following experimental traumatic brain injury. Brain, behavior, and immunity 58:291-309. doi:10.1016/j.bbi.2016.07.158
13. Geng L, Fan LM, Liu F, Smith C, Li J (2020) Nox2 dependent redox-regulation of microglial response to amyloid-beta stimulation and microgliosis in aging. Scientific reports 10 (1):1582. doi:10.1038/s41598-020-58422-8
14. Percario S, Moreira DR, Gomes BA, Ferreira ME, Goncalves AC, Laurindo PS, Vilhena TC, Dolabela MF, Green MD (2012) Oxidative stress in malaria. International journal of molecular sciences 13 (12):16346-16372. doi:10.3390/ijms131216346
15. Imai T, Iwawaki T, Akai R, Suzue K, Hirai M, Taniguchi T, Okada H, Hisaeda H (2014) Evaluating experimental cerebral malaria using oxidative stress indicator OKD48 mice. International journal for parasitology 44 (10):681-685. doi:10.1016/j.ijpara.2014.06.002
16. Reis PA, Comim CM, Hermani F, Silva B, Barichello T, Portella AC, Gomes FC, Sab IM, Frutuoso VS, Oliveira MF, Bozza PT, Bozza FA, Dal-Pizzol F, Zimmerman GA, Quevedo J, Castro-Faria-Neto HC (2010) Cognitive dysfunction is sustained after rescue therapy in experimental cerebral malaria, and is reduced by additive antioxidant therapy. PLoS pathogens 6 (6):e1000963. doi:10.1371/journal.ppat.1000963
17. Laverse E, Nashef L, Brown S (2013) Neurocognitive sequelae following hippocampal and callosal lesions associated with cerebral malaria in an immune-naive adult. Postgraduate medical journal 89 (1057):671-672. doi:10.1136/postgradmedj-2013-131758
18. Kim JY, Park J, Lee JE, Yenari MA (2017) NOX Inhibitors - A Promising Avenue for Ischemic Stroke. Experimental neurobiology 26 (4):195-205. doi:10.5607/en.2017.26.4.195
19. Maraldi T (2013) Natural compounds as modulators of NADPH oxidases. Oxidative medicine and cellular longevity 2013:271602. doi:10.1155/2013/271602
20. Yang T, Zang DW, Shan W, Guo AC, Wu JP, Wang YJ, Wang Q (2019) Synthesis and Evaluations of Novel Apocynin Derivatives as Anti-Glioma Agents. Frontiers in pharmacology 10:951. doi:10.3389/fphar.2019.00951
21. McIntosh HM, Olliaro P (2000) Artemisinin derivatives for treating severe malaria. The Cochrane database of systematic reviews (2):CD000527. doi:10.1002/14651858.CD000527
22. Li Q, Weina P (2010) Artesunate: The Best Drug in the Treatment of Severe and Complicated Malaria. Pharmaceuticals (Basel) 3 (7):2322-2332. doi:10.3390/ph3072322
23. Bouet V, Boulouard M, Toutain J, Divoux D, Bernaudin M, Schumann-Bard P, Freret T (2009) The adhesive removal test: a sensitive method to assess sensorimotor deficits in mice. Nature protocols 4 (10):1560-1564. doi:10.1038/nprot.2009.125
24. Freret T, Bouet V, Leconte C, Roussel S, Chazalviel L, Divoux D, Schumann-Bard P, Boulouard M (2009) Behavioral deficits after distal focal cerebral ischemia in mice: Usefulness of adhesive removal test. Behavioral neuroscience 123 (1):224-230. doi:10.1037/a0014157

25. Balkaya M, Krober JM, Rex A, Endres M (2013) Assessing post-stroke behavior in mouse models of focal ischemia. Journal of cerebral blood flow and metabolism : official journal of the International Society of Cerebral Blood Flow and Metabolism 33 (3):330-338. doi:10.1038/jcbfm.2012.185
26. Fleming SM, Ekhator OR, Ghisays V (2013) Assessment of sensorimotor function in mouse models of Parkinson's disease. Journal of visualized experiments : JoVE (76). doi:10.3791/50303
27. Luong TN, Carlisle HJ, Southwell A, Patterson PH (2011) Assessment of motor balance and coordination in mice using the balance beam. Journal of visualized experiments : JoVE (49). doi:10.3791/2376
28. Wahl D, Coogan SC, Solon-Biet SM, de Cabo R, Haran JB, Raubenheimer D, Cogger VC, Mattson MP, Simpson SJ, Le Couteur DG (2017) Cognitive and behavioral evaluation of nutritional interventions in rodent models of brain aging and dementia. Clinical interventions in aging 12:1419-1428. doi:10.2147/CIA.S145247
29. Gawel K, Gibula E, Marszalek-Grabska M, Filarowska J, Kotlinska JH (2019) Assessment of spatial learning and memory in the Barnes maze task in rodents-methodological consideration. Naunyn-Schmiedeberg's archives of pharmacology 392 (1):1-18. doi:10.1007/s00210-018-1589-y
30. Deacon RM, Rawlins JN (2006) T-maze alternation in the rodent. Nature protocols 1 (1):7-12. doi:10.1038/nprot.2006.2
31. Davis KE, Burnett K, Gigg J (2017) Water and T-maze protocols are equally efficient methods to assess spatial memory in 3xTg Alzheimer's disease mice. Behavioural brain research 331:54-66. doi:10.1016/j.bbr.2017.05.005
32. Medawar E, Benway TA, Liu W, Hanan TA, Haslehurst P, James OT, Yap K, Muessig L, Moroni F, Nahaboo Solim MA, Baidildinova G, Wang R, Richardson JC, Cacucci F, Salih DA, Cummings DM, Edwards FA (2019) Effects of rising amyloidbeta levels on hippocampal synaptic transmission, microglial response and cognition in APPSwe/PSEN1M146V transgenic mice. EBioMedicine 39:422-435. doi:10.1016/j.ebiom.2018.12.006
33. Lueptow LM (2017) Novel Object Recognition Test for the Investigation of Learning and Memory in Mice. Journal of visualized experiments : JoVE (126). doi:10.3791/55718
34. Bian GL, Wei LC, Shi M, Wang YQ, Cao R, Chen LW (2007) Fluoro-Jade C can specifically stain the degenerative neurons in the substantia nigra of the 1-methyl-4-phenyl-1,2,3,6-tetrahydro pyridine-treated C57BL/6 mice. Brain research 1150:55-61. doi:10.1016/j.brainres.2007.02.078
35. Feldman AT, Wolfe D (2014) Tissue processing and hematoxylin and eosin staining. Methods Mol Biol 1180:31-43. doi:10.1007/978-1-4939-1050-2_3
36. Alturkistani HA, Tashkandi FM, Mohammedsaleh ZM (2015) Histological Stains: A Literature Review and Case Study. Global journal of health science 8 (3):72-79. doi:10.5539/gjhs.v8n3p72
37. Cardiff RD, Miller CH, Munn RJ (2014) Manual hematoxylin and eosin staining of mouse tissue sections. Cold Spring Harbor protocols 2014 (6):655-658. doi:10.1101/pdb.prot073411
38. Martins YC, Freeman BD, Akide Ndunge OB, Weiss LM, Tanowitz HB, Desruisseaux MS (2016) Endothelin-1 Treatment Induces an Experimental Cerebral Malaria-Like Syndrome in C57BL/6 Mice Infected with Plasmodium berghei NK65. The American journal of pathology 186 (11):2957-2969. doi:10.1016/j.ajpath.2016.07.020
39. Zaqout S, Kaindl AM (2016) Golgi-Cox Staining Step by Step. Frontiers in neuroanatomy 10:38. doi:10.3389/fnana.2016.00038

40. Wilson MD, Sethi S, Lein PJ, Keil KP (2017) Valid statistical approaches for analyzing sholl data: Mixed effects versus simple linear models. Journal of neuroscience methods 279:33-43. doi:10.1016/j.jneumeth.2017.01.003
41. Nishanth G, Schluter D (2019) Blood-Brain Barrier in Cerebral Malaria: Pathogenesis and Therapeutic Intervention. Trends in parasitology 35 (7):516-528. doi:10.1016/j.pt.2019.04.010
42. Shikani HJ, Freeman BD, Lisanti MP, Weiss LM, Tanowitz HB, Desruisseaux MS (2012) Cerebral malaria: we have come a long way. The American journal of pathology 181 (5):1484-1492. doi:10.1016/j.ajpath.2012.08.010
43. Nag S (2003) Blood-brain barrier permeability using tracers and immunohistochemistry. Methods in molecular medicine 89:133-144. doi:10.1385/1-59259-419-0:133
44. Yuan F, Salehi HA, Boucher Y, Vasthare US, Tuma RF, Jain RK (1994) Vascular permeability and microcirculation of gliomas and mammary carcinomas transplanted in rat and mouse cranial windows. Cancer research 54 (17):4564-4568
45. Sorce S, Stocker R, Seredenina T, Holmdahl R, Aguzzi A, Chio A, Depaulis A, Heitz F, Olofsson P, Olsson T, Duveau V, Sanoudou D, Skosgater S, Vlahou A, Wasquel D, Krause KH, Jaquet V (2017) NADPH oxidases as drug targets and biomarkers in neurodegenerative diseases: What is the evidence? Free radical biology & medicine 112:387-396. doi:10.1016/j.freeradbiomed.2017.08.006
46. Postma NS, Zuidema J, Mommérs EC, Eling WMC (1996) Oxidative stress in malaria; implications for prevention and therapy. Pharmacy World and Science 18 (4):121-129. doi:10.1007/bf00717727
47. DellaValle B, Hempel C, Staalsoe T, Johansen FF, Kurtzhals JAL (2016) Erratum to: Glucagon-like peptide-1 analogue, liraglutide, in experimental cerebral malaria: implications for the role of oxidative stress in cerebral malaria. Malaria journal 15:495. doi:10.1186/s12936-016-1544-7
48. Clark IA, Ilschner S, MacMicking JD, Cowden WB (1990) TNF and Plasmodium berghei ANKA-induced cerebral malaria. Immunology letters 25 (1-3):195-198. doi:10.1016/0165-2478(90)90114-6
49. Sugawara T, Lewen A, Noshita N, Gasche Y, Chan PH (2002) Effects of global ischemia duration on neuronal, astroglial, oligodendroglial, and microglial reactions in the vulnerable hippocampal CA1 subregion in rats. Journal of neurotrauma 19 (1):85-98. doi:10.1089/089771502753460268
50. Davoli MA, Fourtounis J, Tam J, Xanthoudakis S, Nicholson D, Robertson GS, Ng GY, Xu D (2002) Immunohistochemical and biochemical assessment of caspase-3 activation and DNA fragmentation following transient focal ischemia in the rat. Neuroscience 115 (1):125-136. doi:10.1016/s0306-4522(02)00376-7
51. McPhail LT, McBride CB, McGraw J, Steeves JD, Tetzlaff W (2004) Axotomy abolishes NeuN expression in facial but not rubrospinal neurons. Experimental neurology 185 (1):182-190. doi:10.1016/j.expneurol.2003.10.001
52. Fischer R, Maier O (2015) Interrelation of oxidative stress and inflammation in neurodegenerative disease: role of TNF. Oxidative medicine and cellular longevity 2015:610813. doi:10.1155/2015/610813
53. Head E (2009) Oxidative damage and cognitive dysfunction: antioxidant treatments to promote healthy brain aging. Neurochemical research 34 (4):670-678. doi:10.1007/s11064-008-9808-4
54. Pratico D, Clark CM, Liun F, Rokach J, Lee VY, Trojanowski JQ (2002) Increase of brain oxidative stress in mild cognitive impairment: a possible predictor of Alzheimer disease. Archives of neurology 59 (6):972-976.

doi:10.1001/archneur.59.6.972

55. Agostinho P, Cunha RA, Oliveira C (2010) Neuroinflammation, oxidative stress and the pathogenesis of Alzheimer's disease. Current pharmaceutical design 16 (25):2766-2778. doi:10.2174/138161210793176572
56. Solleiro-Villavicencio H, Rivas-Arancibia S (2018) Effect of Chronic Oxidative Stress on Neuroinflammatory Response Mediated by CD4(+)T Cells in Neurodegenerative Diseases. Frontiers in cellular neuroscience 12:114. doi:10.3389/fncel.2018.00114
57. Medana IM, Turner GD (2006) Human cerebral malaria and the blood-brain barrier. International journal for parasitology 36 (5):555-568. doi:10.1016/j.ijpara.2006.02.004
58. Investigators M-EN (2018) Early childhood cognitive development is affected by interactions among illness, diet, enteropathogens and the home environment: findings from the MAL-ED birth cohort study. BMJ global health 3 (4):e000752. doi:10.1136/bmjgh-2018-000752
59. Anand KS, Dhikav V (2012) Hippocampus in health and disease: An overview. Annals of Indian Academy of Neurology 15 (4):239-246. doi:10.4103/0972-2327.104323
60. Moodley KK, Chan D (2014) The hippocampus in neurodegenerative disease. Frontiers of neurology and neuroscience 34:95-108. doi:10.1159/000356430
61. Huttenrauch M, Brauss A, Kurdakova A, Borgers H, Klinker F, Liebetanz D, Salinas-Riester G, Wiltfang J, Klafki HW, Wirths O (2016) Physical activity delays hippocampal neurodegeneration and rescues memory deficits in an Alzheimer disease mouse model. Translational psychiatry 6:e800. doi:10.1038/tp.2016.65
62. Kihara M, Carter JA, Holding PA, Vargha-Khadem F, Scott RC, Idro R, Fegan GW, de Haan M, Neville BG, Newton CR (2009) Impaired everyday memory associated with encephalopathy of severe malaria: the role of seizures and hippocampal damage. Malaria journal 8:273. doi:10.1186/1475-2875-8-273
63. Langfitt JT, McDermott MP, Brim R, Mboma S, Potchen MJ, Kampondeni SD, Seydel KB, Semrud-Clikeman M, Taylor TE (2019) Neurodevelopmental Impairments 1 Year After Cerebral Malaria. Pediatrics 143 (2). doi:10.1542/peds.2018-1026
64. Idro R, Jenkins NE, Newton CR (2005) Pathogenesis, clinical features, and neurological outcome of cerebral malaria. The Lancet Neurology 4 (12):827-840. doi:10.1016/S1474-4422(05)70247-7
65. Lillemoe K, Brewington D, Lord A, Czeisler B, Lewis A, Kurzweil A (2019) Teaching NeuroImages: Hippocampal sclerosis in cerebral malaria. Neurology 93 (1):e112-e113. doi:10.1212/WNL.0000000000007725
66. Wilson C, Nunez MT, Gonzalez-Billault C (2015) Contribution of NADPH oxidase to the establishment of hippocampal neuronal polarity in culture. Journal of cell science 128 (16):2989-2995. doi:10.1242/jcs.168567
67. Tejada-Simon MV, Serrano F, Villasana LE, Kanterewicz BI, Wu GY, Quinn MT, Klann E (2005) Synaptic localization of a functional NADPH oxidase in the mouse hippocampus. Molecular and cellular neurosciences 29 (1):97-106. doi:10.1016/j.mcn.2005.01.007
68. Di Filippo M, de Iure A, Giampa C, Chiasserini D, Tozzi A, Orvietani PL, Ghiglieri V, Tantucci M, Durante V, Quiroga-Varela A, Mancini A, Costa C, Sarchielli P, Fusco FR, Calabresi P (2016) Persistent activation of microglia and NADPH oxidase [corrected] drive hippocampal dysfunction in experimental multiple sclerosis. Scientific reports 6:20926. doi:10.1038/srep20926

69. Ma MW, Wang J, Zhang Q, Wang R, Dhandapani KM, Vadlamudi RK, Brann DW (2017) NADPH oxidase in brain injury and neurodegenerative disorders. Molecular neurodegeneration 12 (1):7. doi:10.1186/s13024-017-0150-7
70. Ansari MA, Scheff SW (2011) NADPH-oxidase activation and cognition in Alzheimer disease progression. Free radical biology & medicine 51 (1):171-178. doi:10.1016/j.freeradbiomed.2011.03.025
71. Valencia A, Sapp E, Kimm JS, McClory H, Reeves PB, Alexander J, Ansong KA, Masso N, Frosch MP, Kegel KB, Li X, DiFiglia M (2013) Elevated NADPH oxidase activity contributes to oxidative stress and cell death in Huntington's disease. Human molecular genetics 22 (6):1112-1131. doi:10.1093/hmg/dds516
72. Wu DC, Re DB, Nagai M, Ischiropoulos H, Przedborski S (2006) The inflammatory NADPH oxidase enzyme modulates motor neuron degeneration in amyotrophic lateral sclerosis mice. Proceedings of the National Academy of Sciences of the United States of America 103 (32):12132-12137. doi:10.1073/pnas.0603670103
73. Belarbi K, Cuvelier E, Destee A, Gressier B, Chartier-Harlin MC (2017) NADPH oxidases in Parkinson's disease: a systematic review. Molecular neurodegeneration 12 (1):84. doi:10.1186/s13024-017-0225-5
74. Francischetti IM, Gordon E, Bizzarro B, Gera N, Andrade BB, Oliveira F, Ma D, Assumpcao TC, Ribeiro JM, Pena M, Qi CF, Diouf A, Moretz SE, Long CA, Ackerman HC, Pierce SK, Sa-Nunes A, Waisberg M (2014) Tempol, an intracellular antioxidant, inhibits tissue factor expression, attenuates dendritic cell function, and is partially protective in a murine model of cerebral malaria. PloS one 9 (2):e87140. doi:10.1371/journal.pone.0087140
75. Sanni LA, Fu S, Dean RT, Bloomfield G, Stocker R, Chaudhri G, Dinauer MC, Hunt NH (1999) Are reactive oxygen species involved in the pathogenesis of murine cerebral malaria? The Journal of infectious diseases 179 (1):217-222. doi:10.1086/314552
76. Potter SM, Mitchell AJ, Cowden WB, Sanni LA, Dinauer M, de Haan JB, Hunt NH (2005) Phagocyte-derived reactive oxygen species do not influence the progression of murine blood-stage malaria infections. Infection and immunity 73 (8):4941-4947. doi:10.1128/IAI.73.8.4941-4947.2005
77. Kuriakose M, Younger D, Ravula AR, Alay E, Rama Rao KV, Chandra N (2019) Synergistic Role of Oxidative Stress and Blood-Brain Barrier Permeability as Injury Mechanisms in the Acute Pathophysiology of Blast-induced Neurotrauma. Scientific reports 9 (1):7717. doi:10.1038/s41598-019-44147-w
78. Casas AI, Geuss E, Kleikers PWM, Mencl S, Herrmann AM, Buendia I, Egea J, Meuth SG, Lopez MG, Kleinschnitz C, Schmidt H (2017) NOX4-dependent neuronal autotoxicity and BBB breakdown explain the superior sensitivity of the brain to ischemic damage. Proceedings of the National Academy of Sciences of the United States of America 114 (46):12315-12320. doi:10.1073/pnas.1705034114
79. Casas AI, Kleikers PW, Geuss E, Langhauser F, Adler T, Busch DH, Gailus-Durner V, de Angelis MH, Egea J, Lopez MG, Kleinschnitz C, Schmidt HH (2019) Calcium-dependent blood-brain barrier breakdown by NOX5 limits postreperfusion benefit in stroke. The Journal of clinical investigation 129 (4):1772-1778. doi:10.1172/JCI124283
80. John CC, Kutamba E, Mugarura K, Opoka RO (2010) Adjunctive therapy for cerebral malaria and other severe forms of Plasmodium falciparum malaria. Expert review of anti-infective therapy 8 (9):997-1008. doi:10.1586/eri.10.90
81. Varo R, Crowley VM, Sitoe A, Madrid L, Serghides L, Kain KC, Bassat Q (2018) Adjunctive therapy for severe malaria: a review and critical appraisal. Malaria journal 17 (1):47. doi:10.1186/s12936-018-2195-7

82. Jackman KA, Miller AA, De Silva TM, Crack PJ, Drummond GR, Sobey CG (2009) Reduction of cerebral infarct volume by apocynin requires pretreatment and is absent in Nox2-deficient mice. British journal of pharmacology 156 (4):680-688. doi:10.1111/j.1476-5381.2008.00073.x
83. Paterniti I, Galuppo M, Mazzon E, Impellizzeri D, Esposito E, Bramanti P, Cuzzocrea S (2010) Protective effects of apocynin, an inhibitor of NADPH oxidase activity, in splanchnic artery occlusion and reperfusion. Journal of leukocyte biology 88 (5):993-1003. doi:10.1189/jlb.0610322
84. Tang XN, Cairns B, Cairns N, Yenari MA (2008) Apocynin improves outcome in experimental stroke with a narrow dose range. Neuroscience 154 (2):556-562. doi:10.1016/j.neuroscience.2008.03.090
85. Choi BY, Jang BG, Kim JH, Lee BE, Sohn M, Song HK, Suh SW (2012) Prevention of traumatic brain injury-induced neuronal death by inhibition of NADPH oxidase activation. Brain research 1481:49-58. doi:10.1016/j.brainres.2012.08.032
86. Lu XY, Wang HD, Xu JG, Ding K, Li T (2014) NADPH oxidase inhibition improves neurological outcome in experimental traumatic brain injury. Neurochemistry international 69:14-19. doi:10.1016/j.neuint.2014.02.006
87. Lu BW, Baum L, So KF, Chiu K, Xie LK (2019) More than anti-malarial agents: therapeutic potential of artemisinins in neurodegeneration. Neural regeneration research 14 (9):1494-1498. doi:10.4103/1673-5374.255960
88. Li S, Zhao X, Lazarovici P, Zheng W (2019) Artemether Activation of AMPK/GSK3beta(ser9)/Nrf2 Signaling Confers Neuroprotection towards beta-Amyloid-Induced Neurotoxicity in 3xTg Alzheimer's Mouse Model. Oxidative medicine and cellular longevity 2019:1862437. doi:10.1155/2019/1862437
89. Okorji UP, Velagapudi R, El-Bakoush A, Fiebich BL, Olajide OA (2016) Antimalarial Drug Artemether Inhibits Neuroinflammation in BV2 Microglia Through Nrf2-Dependent Mechanisms. Molecular neurobiology 53 (9):6426-6443. doi:10.1007/s12035-015-9543-1
90. Antoine T, Fisher N, Amewu R, O'Neill PM, Ward SA, Biagini GA (2014) Rapid kill of malaria parasites by artemisinin and semi-synthetic endoperoxides involves ROS-dependent depolarization of the membrane potential. The Journal of antimicrobial chemotherapy 69 (4):1005-1016. doi:10.1093/jac/dkt486
91. Kavishe RA, Koenderink JB, Alifrangis M (2017) Oxidative stress in malaria and artemisinin combination therapy: Pros and Cons. The FEBS journal 284 (16):2579-2591. doi:10.1111/febs.14097
92. Gopalakrishnan AM, Kumar N (2015) Antimalarial action of artesunate involves DNA damage mediated by reactive oxygen species. Antimicrobial agents and chemotherapy 59 (1):317-325. doi:10.1128/AAC.03663-14
93. Kulkarni VA, Firestein BL (2012) The dendritic tree and brain disorders. Molecular and cellular neurosciences 50 (1):10-20. doi:10.1016/j.mcn.2012.03.005
94. Lopez-Domenech G, Higgs NF, Vaccaro V, Ros H, Arancibia-Carcamo IL, MacAskill AF, Kittler JT (2016) Loss of Dendritic Complexity Precedes Neurodegeneration in a Mouse Model with Disrupted Mitochondrial Distribution in Mature Dendrites. Cell reports 17 (2):317-327. doi:10.1016/j.celrep.2016.09.004
95. Kweon JH, Kim S, Lee SB (2017) The cellular basis of dendrite pathology in neurodegenerative diseases. BMB reports 50 (1):5-11. doi:10.5483/bmbrep.2017.50.1.131
96. Tang FL, Zhao L, Zhao Y, Sun D, Zhu XJ, Mei L, Xiong WC (2020) Coupling of terminal differentiation deficit with neurodegenerative pathology in Vps35-deficient pyramidal neurons. Cell death and differentiation 27

(7):2099-2116. doi:10.1038/s41418-019-0487-2

97. Kapoor M, Sharma N, Sandhir R, Nehru B (2018) Effect of the NADPH oxidase inhibitor apocynin on ischemia-reperfusion hippocampus injury in rat brain. Biomedicine & pharmacotherapy = Biomedecine & pharmacotherapie 97:458-472. doi:10.1016/j.biopha.2017.10.123
98. Bartsch T, Dohring J, Reuter S, Finke C, Rohr A, Brauer H, Deuschl G, Jansen O (2015) Selective neuronal vulnerability of human hippocampal CA1 neurons: lesion evolution, temporal course, and pattern of hippocampal damage in diffusion-weighted MR imaging. Journal of cerebral blood flow and metabolism : official journal of the International Society of Cerebral Blood Flow and Metabolism 35 (11):1836-1845. doi:10.1038/jcbfm.2015.137
99. Parastan RH, Christopher M, Torrys YS, Mahadewa TGB (2020) Combined Therapy Potential of Apocynin and Tert-butylhydroquinone as a Therapeutic Agent to Prevent Secondary Progression to Traumatic Brain Injury. Asian journal of neurosurgery 15 (1):10-15. doi:10.4103/ajns.AJNS_231_19
100. Lee SH, Choi BY, Kho AR, Jeong JH, Hong DK, Kang DH, Kang BS, Song HK, Choi HC, Suh SW (2018) Inhibition of NADPH Oxidase Activation by Apocynin Rescues Seizure-Induced Reduction of Adult Hippocampal Neurogenesis. International journal of molecular sciences 19 (10). doi:10.3390/ijms19103087
101. Dang DK, Shin EJ, Nam Y, Ryoo S, Jeong JH, Jang CG, Nabeshima T, Hong JS, Kim HC (2016) Apocynin prevents mitochondrial burdens, microglial activation, and pro-apoptosis induced by a toxic dose of methamphetamine in the striatum of mice via inhibition of p47phox activation by ERK. Journal of neuroinflammation 13:12. doi:10.1186/s12974-016-0478-x
102. Merlini M, Rafalski VA, Rios Coronado PE, Gill TM, Ellisman M, Muthukumar G, Subramanian KS, Ryu JK, Syme CA, Davalos D, Seeley WW, Mucke L, Nelson RB, Akassoglou K (2019) Fibrinogen Induces Microglia-Mediated Spine Elimination and Cognitive Impairment in an Alzheimer's Disease Model. Neuron 101 (6):1099-1108 e1096. doi:10.1016/j.neuron.2019.01.014
103. Hou L, Sun F, Huang R, Sun W, Zhang D, Wang Q (2019) Inhibition of NADPH oxidase by apocynin prevents learning and memory deficits in a mouse Parkinson's disease model. Redox biology 22:101134. doi:10.1016/j.redox.2019.101134
104. Kumar SP, Babu PP (2020) Aberrant Dopamine Receptor Signaling Plays Critical Role in the Impairment of Striatal Neurons in Experimental Cerebral Malaria. Molecular neurobiology 57 (12):5069-5083. doi:10.1007/s12035-020-02076-0
105. Olumese PE, Bjorkman A, Gbadegesin RA, Adeyemo AA, Walker O (1999) Comparative efficacy of intramuscular artemether and intravenous quinine in Nigerian children with cerebral malaria. Acta tropica 73 (3):231-236. doi:10.1016/s0001-706x(99)00031-5
106. van Hensbroek MB, Palmer A, Jaffar S, Schneider G, Kwiatkowski D (1997) Residual neurologic sequelae after childhood cerebral malaria. The Journal of pediatrics 131 (1 Pt 1):125-129. doi:10.1016/s0022-3476(97)70135-5
107. Walker O, Salako LA, Omokhodion SI, Sowunmi A (1993) An open randomized comparative study of intramuscular artemether and intravenous quinine in cerebral malaria in children. Transactions of the Royal Society of Tropical Medicine and Hygiene 87 (5):564-566. doi:10.1016/0035-9203(93)90092-5
108. Bitta MA, Kariuki SM, Mwita C, Gwer S, Mwai L, Newton C (2017) Antimalarial drugs and the prevalence of mental and neurological manifestations: A systematic review and meta-analysis. Wellcome open research 2:13. doi:10.12688/wellcomeopenres.10658.2

109. Dranka BP, Gifford A, McAllister D, Zielonka J, Joseph J, O'Hara CL, Stucky CL, Kanthasamy AG, Kalyanaraman B (2014) A novel mitochondrially-targeted apocynin derivative prevents hyposmia and loss of motor function in the leucine-rich repeat kinase 2 (LRRK2(R1441G)) transgenic mouse model of Parkinson's disease. Neuroscience letters 583:159-164. doi:10.1016/j.neulet.2014.09.042

110. Choi BY, Kim JH, Kho AR, Kim IY, Lee SH, Lee BE, Choi E, Sohn M, Stevenson M, Chung TN, Kauppinen TM, Suh SW (2015) Inhibition of NADPH oxidase activation reduces EAE-induced white matter damage in mice. Journal of neuroinflammation 12:104. doi:10.1186/s12974-015-0325-5

111. Pioli EY, Gaskill BN, Gilmour G, Tricklebank MD, Dix SL, Bannerman D, Garner JP (2014) An automated maze task for assessing hippocampus-sensitive memory in mice. Behavioural brain research 261:249-257. doi:10.1016/j.bbr.2013.12.009

112. Ali SS, Young JW, Wallace CK, Gresack J, Jeste DV, Geyer MA, Dugan LL, Risbrough VB (2011) Initial evidence linking synaptic superoxide production with poor short-term memory in aged mice. Brain research 1368:65-70. doi:10.1016/j.brainres.2010.11.009

Tables

Table.1 Primers used for semi-quantitative PCR.

Gene and GenBank ID:	Forward primer	Reverse primer	Size (bp)	Tm (^{0}C)
Mus musculus Nox2 (Cybb) FJ168469.1	5’-TGGAAACCCTCCTATGACTTG-3’	5’-AACTTGGATACCTTGGGGCAC -3’	216	57.5
GAPDH NM_008084.3	5’-GTGTGAACGGATTTGGCCGTATTG-3’	5-’TTTGCCGTGAGTGGAGTCATACTG -3’	146	58.8

Figures

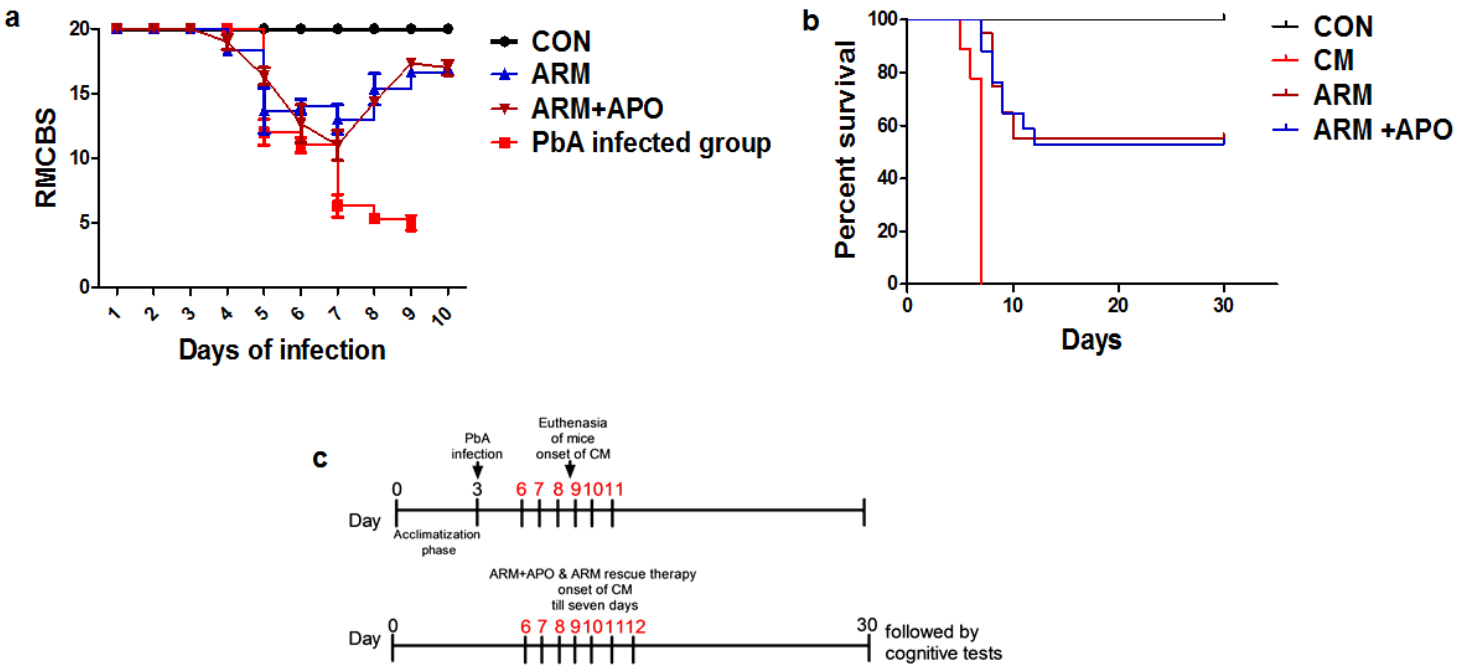

Figure 1

Restoration of neurobehavioral parameters and survivability after rescue therapy onset of CM. a Graph representing a decrease in total RMCBS scores of animals infected with PbA from day 5 to 9 and restoration of behavioral parameters after ARM and ARM+APO adjunctive therapy from day 6 to 10. b Kaplan-Meier survival curve shows a survival percentage of 56 upon ARM treatment and 54 after ARM+APO therapy until a duration of 30 days. Mice infected with PbA were moribund with clinical signs of death due to CM on day 6 and 7. c Work plan representing the time points of CM infection in mice post infected with PbA and corresponding ARM and ARM+APO rescue therapy followed by cognitive tests after a survival phase up to day 30.

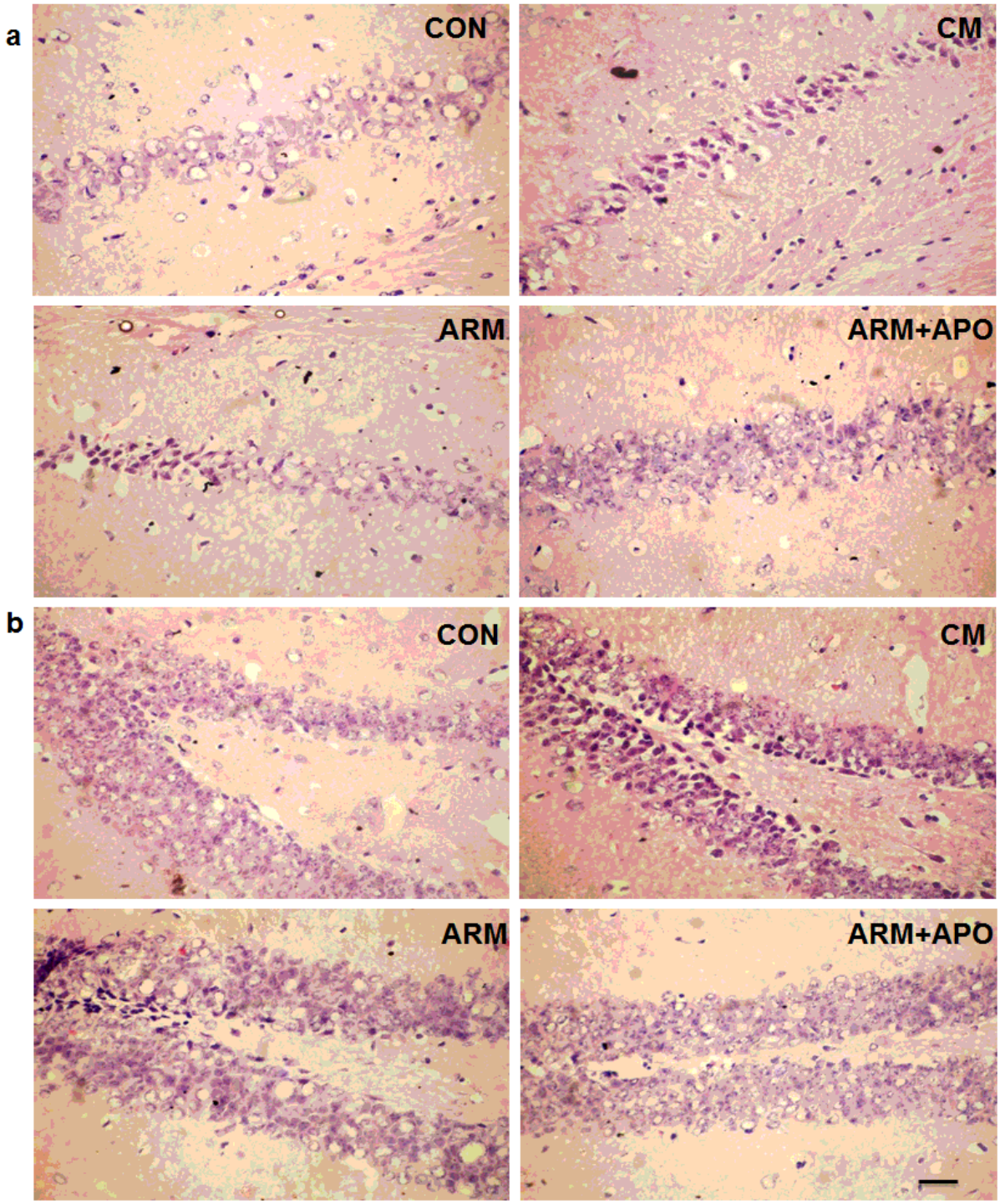

Figure 2

Neuropil deterioration followed by neuroprotection in CA1 and dentate gyrus after APO adjunctive rescue therapy in ECM. a H&E images showing neuropil deterioration with degenerated neurons in CA1 region of hippocampus in CM. Image showing characteristic neurodegeneration in CA1 region despite ARM rescue therapy. Image representing improved neuropil area of CA1 and reduced neuronal damage after APO adjunctive therapy. b Image representing increased neuropil vacuolation in the internal granule layer and hilus of dentate gyrus in CM. Image showing characteristic neuronal death in dentate gyrus in ARM rescue treated brain sections and improved neuropil in dentate gyrus in APO adjunctive therapy. Scale bar = 10 μm.

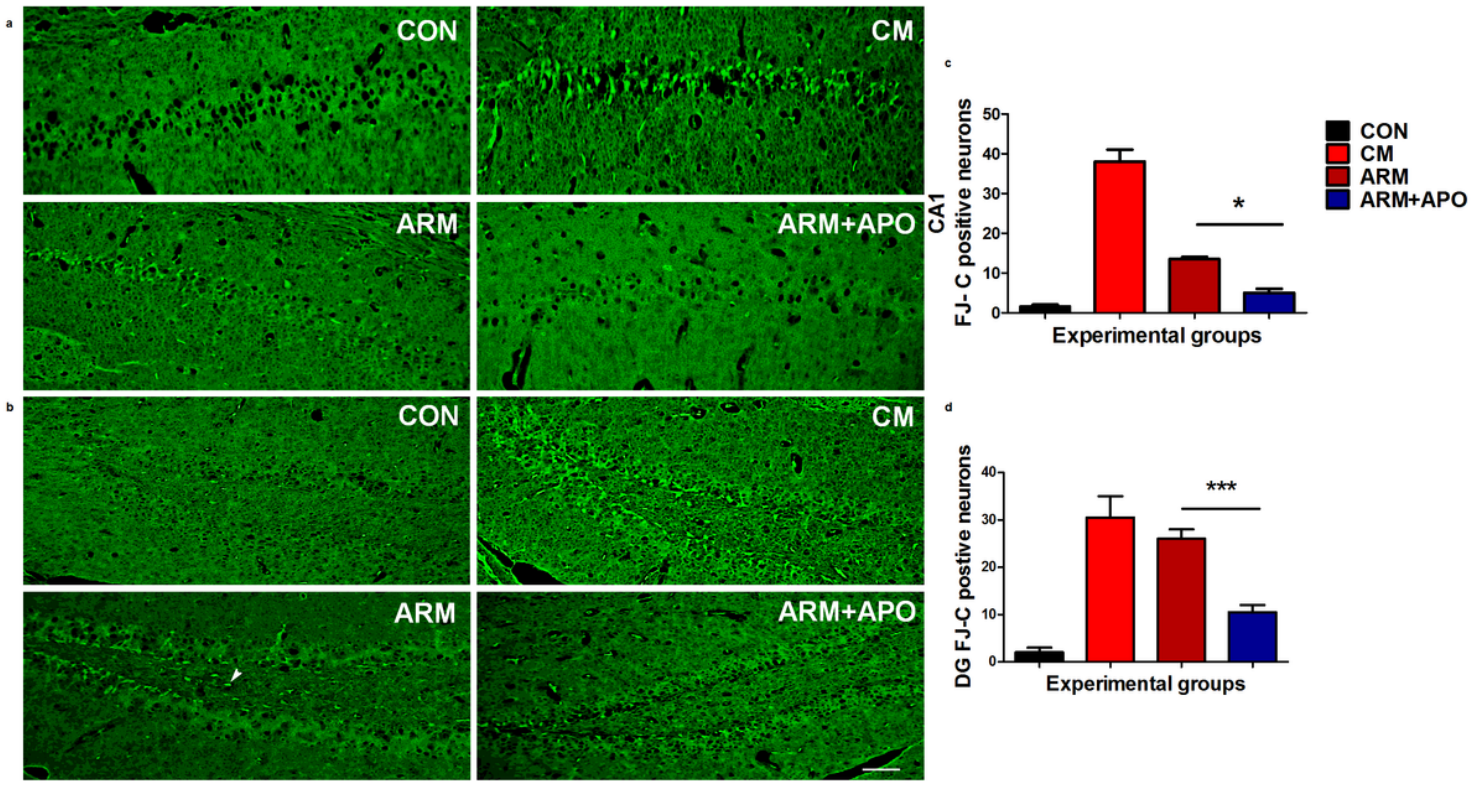

Figure 3

Hippocampal neurodegeneration in ECM. a Fluoro Jade-C stained images representing prominent neurodegeneration in CA1 region and b dentate gyrus in coronal sections of CM (arrowhead showing degenerated neuron in the hilar region of hippocampus). c Graph representing quantification of fluorescence intensities of degenerated neurons in CA1 and d dentate gyrus regions in all the experimental groups. *p<0.05, ***p<0.001 Scale Bar = 10 μm.

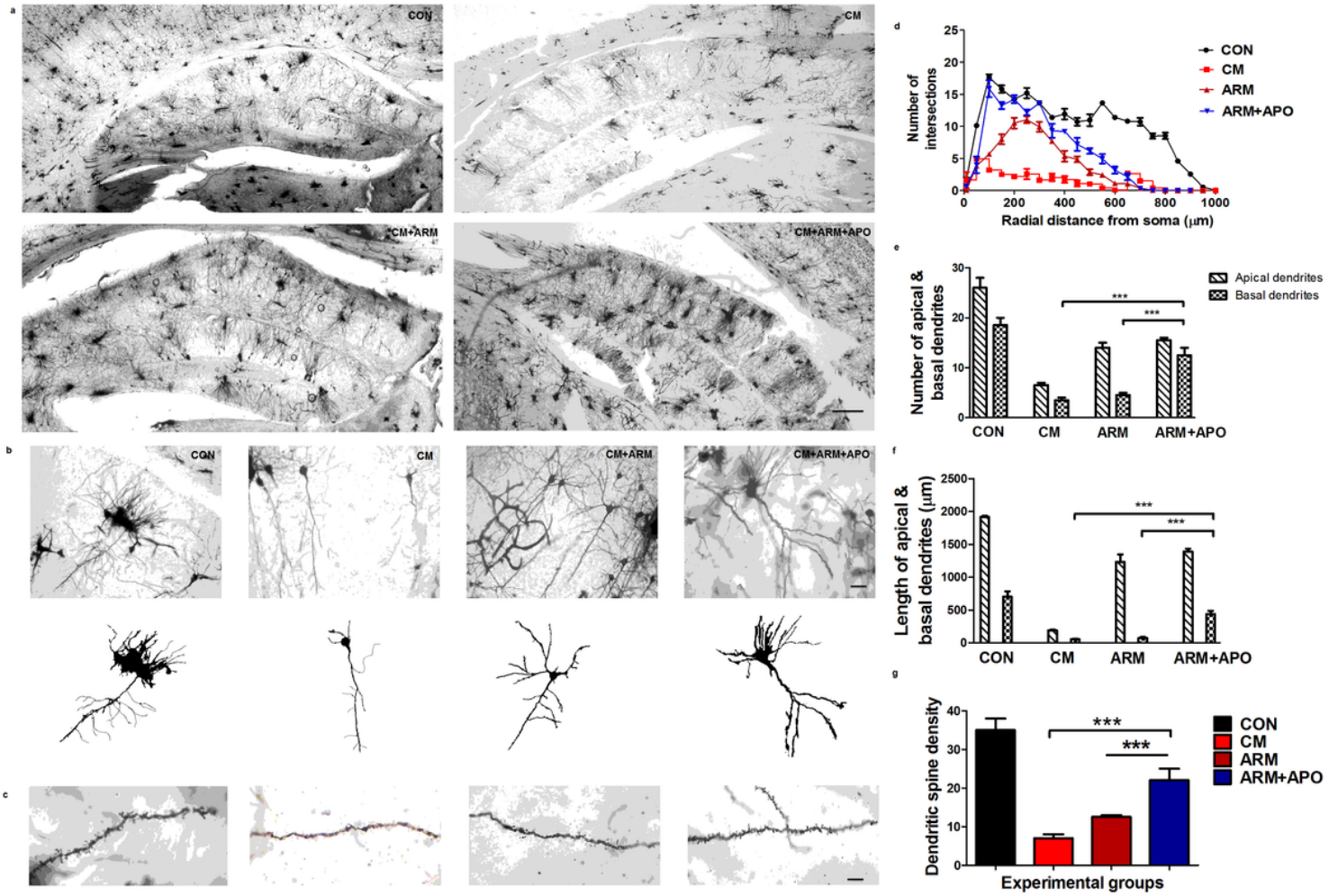

Figure 4

Loss of hippocampal neuronal density in ECM. a Photomicrograph representing Golgi-cox impregnated hippocampal neurons in all the experimental groups. b image representing individual neurons in CA1 region with corresponding skeletonized images c dendritic spines. d graph showing dendritic arborization pattern in CA1 neurons with number of intersections on Y-axis and radial distance from soma on X-axis. e Graph representing the number and f length of apical and basal dendrites of CA1 neurons g Graph representing the dendritic spine density per 10 μm dendrite length. *p<0.05, ***p<0.001 Scale bar = 100 μm (a), 10 μm (b,c)

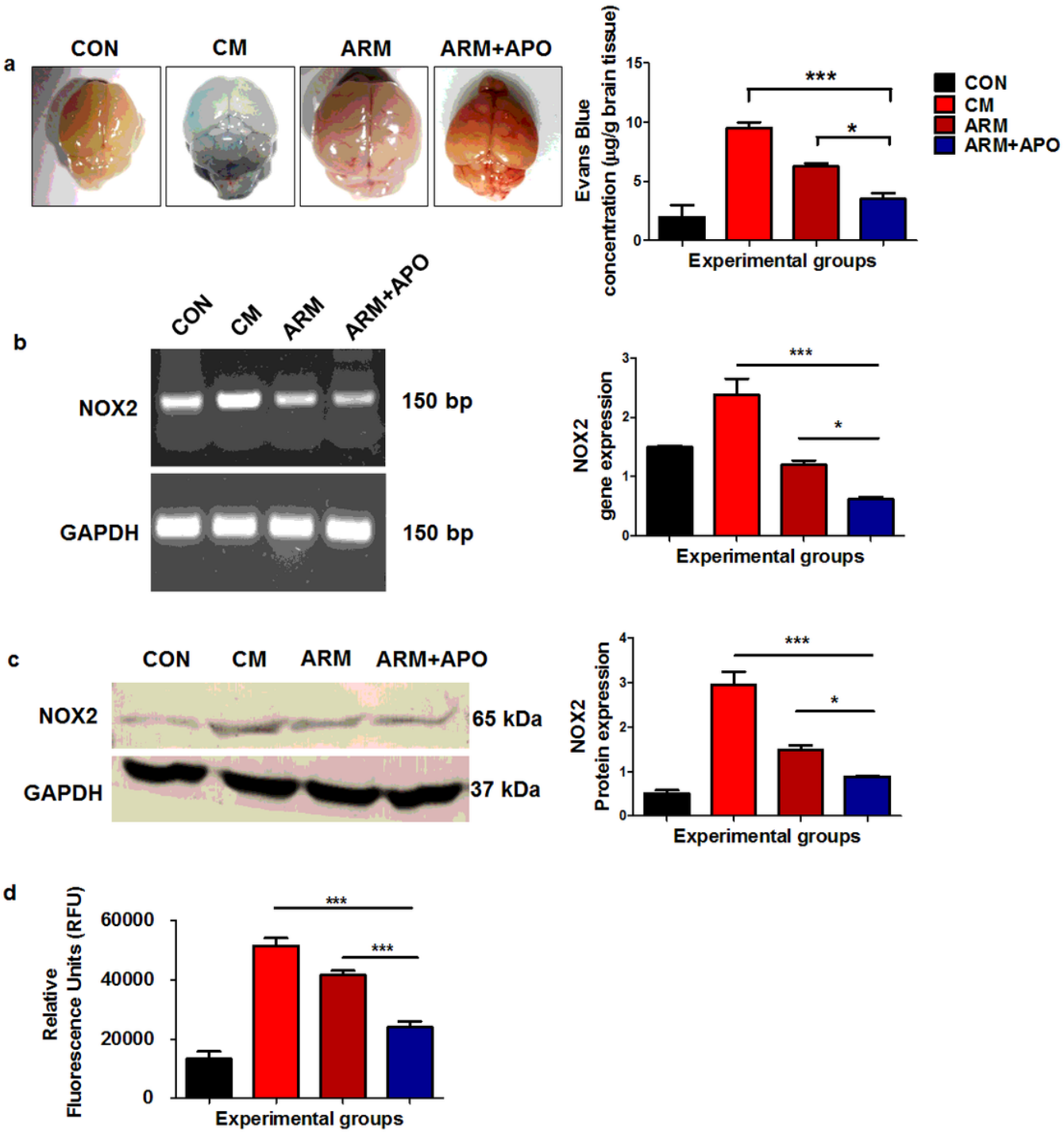

Figure 5

Reduced expression of NOX2 in ECM and restoration of BBB integrity after APO rescue therapy a Image representing appearance of whole brains stained with Evans Blue in all the experimental groups and corresponding graph showing concentrations of Evans Blue dye extravasated. b Image representing NOX2 gene expression and densitometry showing the relative gene levels normalized with GAPDH in the whole brain RNA samples. c Western Blot showing NOX2 protein expression in whole brain lysates with quantification of relative protein levels normalized with GAPDH. d Graph representing quantification of ROS levels by relative fluorescence intensity units in whole brain lysates *p<0.05, ***p<0.001

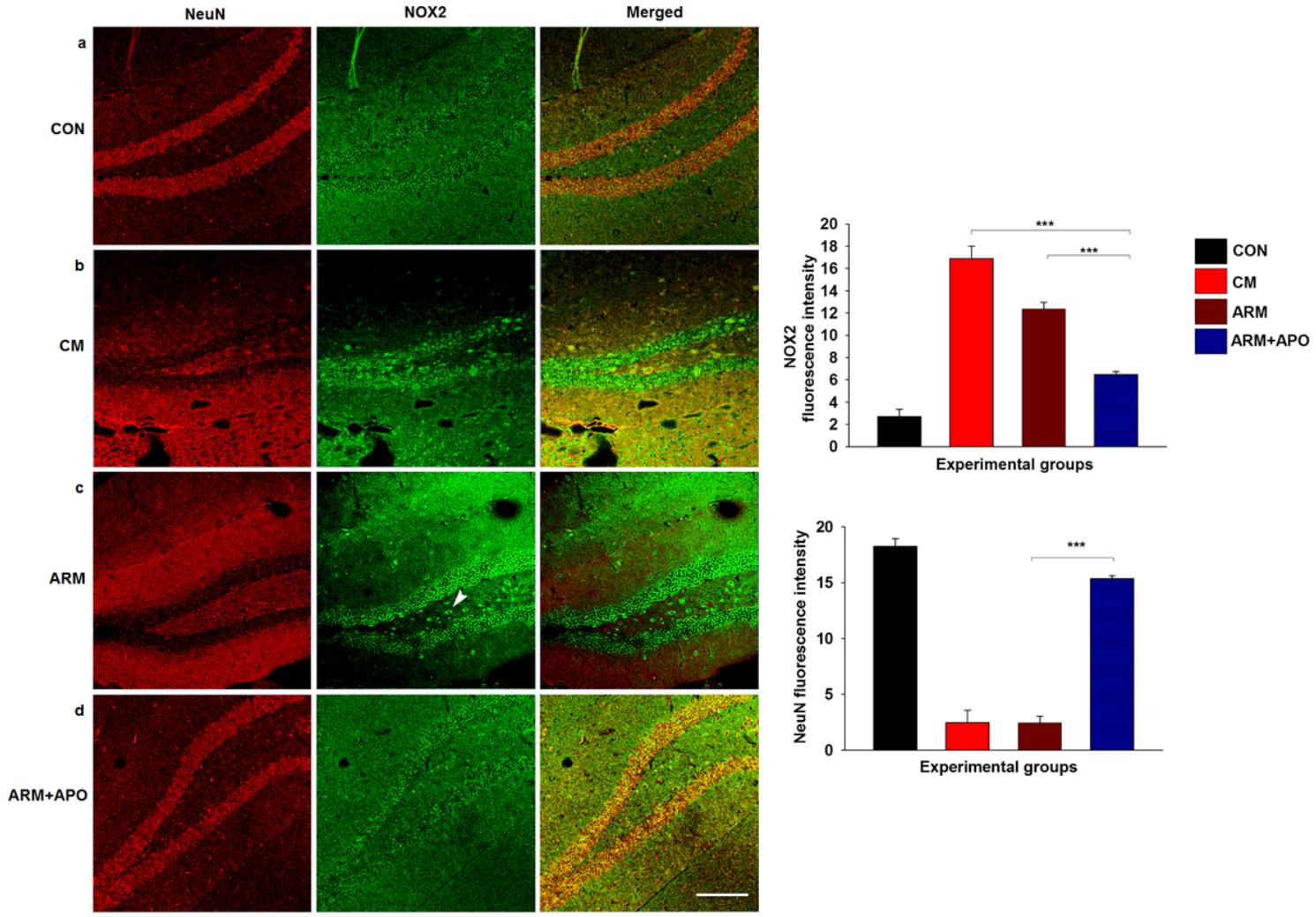

Figure 6

APO adjunctive therapy increased NeuN immunostaining with reduction in NOX2 expression after ECM a Image representing colocalization of NeuN (red) and NOX2 (green) in dentate gyrus of CON brain section. b Loss of NeuN immunoreactivity and increased immunoreactivity of NOX2 in CM infected brain section. c Enhanced immunoreactivity of NOX2 and loss of NeuN staining in ARM treated brain section. d Restoration of NeuN immunostaining and reduction of NOX2 levels in APO adjunctive treated brain section. ***p<0.001 Scale bar= 50 μm

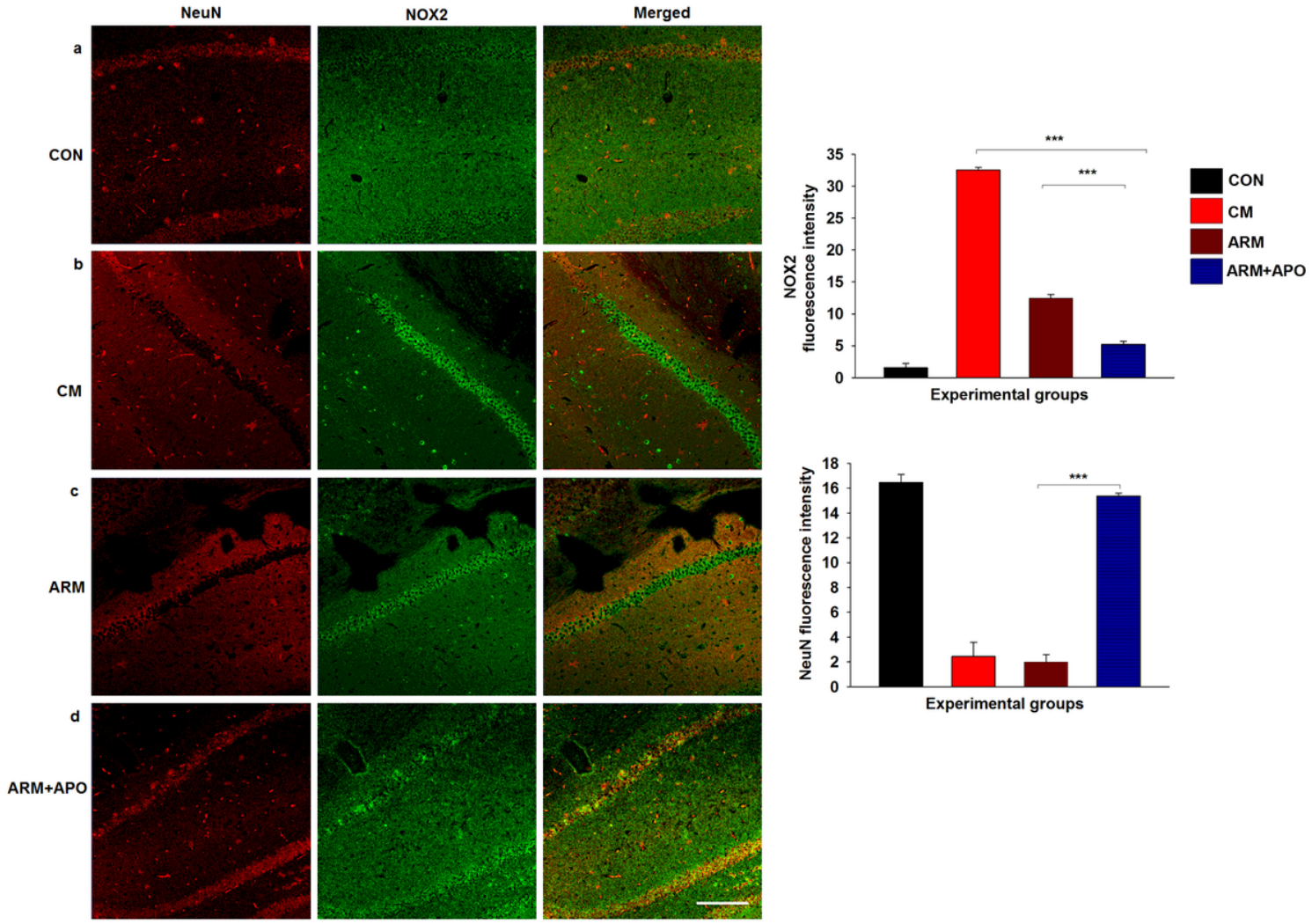

Figure 7

APO adjunctive therapy restored NeuN immunostaining in CA1 region after ECM. a Image representing the immunofluorescence staining of NeuN (red) and significant reduction of NOX2 (green) in CA1 region of CON brain section. b Loss of NeuN staining and increased immunoreactivity of NOX2 in CA1 region of CM infected brain section. c Reduction of NeuN and increased immunoreactivity of NOX2 in ARM treated section. d Restoration of NeuN and reduced NOX2 immunostaining in APO adjunctive treated brain section. ***p<0.001 Scale bar= 50 μm

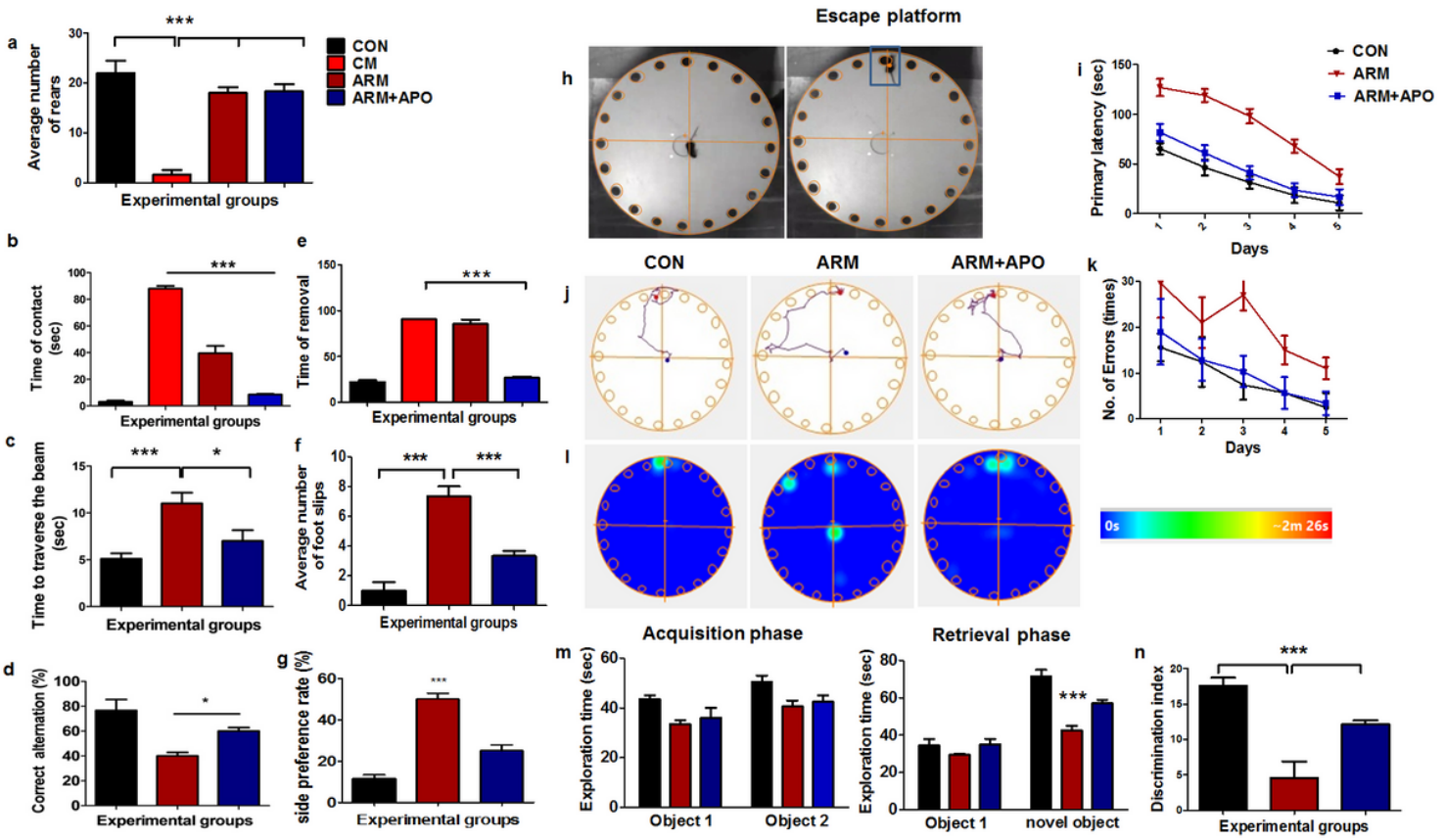

Figure 8

APO adjunctive therapy prevented cognitive impairment after ECM. a Graph representing the average number of rears exhibited by the experimental groups in cylinder test. b,e Graph showing the contact and removal times exhibited in adhesive removal test. c,f Average time for traversal and rate of contralateral foot slipping exhibited in beam balance test. d,g Percentage of correct alternations and side preference rate exhibited in the T-maze test. h Image showing the location of start point of mouse and escape platform in the Barnes maze. j,l Image showing the track plots of the from the start point to the escape platform and heat maps of mouse exhibited in Barnes maze. i,k Graph representing the primary latency and number of errors performed till day 5 (probe trial). m Graph representing the average time spent with object 1 and 2 during the acquisition and retrieval phase in novel object recognition test. n Graph showing the discrimination index exhibited by each experimental group in novel object recognition test. *p<0.05, ***p<0.001

Supplementary Files

This is a list of supplementary files associated with this preprint. Click to download.

- Supplementary1.mp4
- Supplementary2.m4v
- Supplementary3.m4v
- Supplementary4.m4v
- Supplementary5.m4v

- Supplementary6.m4v
- Supplementary7.mp4
- Supplementary8.mp4